Drug Design, Development and Therapy

Dovepress
Taylor & Francis Group

Open Access Full Text Article

ORIGINAL RESEARCH

β-Amyrin Acetate Confers Anti-Epileptic Protection via Suppression of Calcium Overload-Induced Neuroinflammation and Apoptosis

Jiali Cai*, Yaojian Zhang*, Tian Zhang, Mengyi Wu, Dijun Wang, Chunyan Yin, Xueke Nie, Lan Chen, Zhihu Sun, Chanming Liu, Xiaojing Yan

Changzhou Key Laboratory of Human Use Experience Research & Transformation of Menghe Medical School, Changzhou Hospital Affiliated to Nanjing University of Chinese Medicine, Changzhou, People's Republic of China

*These authors contributed equally to this work

Correspondence: Xiaojing Yan, Email yanxiaojing963@njucm.edu.cn

Purpose: β-Amyrin acetate (BAA), a natural pentacyclic triterpenoid, exhibits greater lipophilicity than its antiepileptic precursor β-amyrin, implying enhanced blood-brain barrier (BBB) permeability. This study aimed to evaluate the antiepileptic efficacy of BAA and investigate its neuroprotective mechanisms, with a focus on calcium signaling.

Patients and Methods: An epilepsy model was established in zebrafish using pentylenetetrazole (PTZ) to assess the effects of BAA on seizure-like behaviors, reactive oxygen species (ROS) levels, apoptosis, and inflammatory markers. Potential targets were predicted via network pharmacology and molecular docking. Furthermore, a glutamate (Glu)-induced HT-22 neuronal injury model was used to validate BAA's effects on intracellular calcium homeostasis and downstream signaling pathways.

Results: BAA significantly attenuated PTZ-induced seizure-like behaviors in zebrafish, specifically reducing the frequency of clonic and tonic-clonic seizures, as well as total movement distance and velocity. Concurrently, BAA mitigated oxidative stress, apoptosis, and neuroinflammation in the zebrafish. Network pharmacology and molecular docking analyses suggested the calcium signaling pathway as a potential target, with BAA showing high binding affinity to proteins such as Bcl-2 and JAK2. In vitro experiments suggested that BAA effectively alleviated Glu-induced calcium overload in HT-22 cells. It downregulated the Bax/Bcl-2 ratio, suppressed overactivation of the JAK2/STAT3 pathway, and consequently reduced neuronal apoptosis and inflammation. The BAPTA-AM co-treatment experiment further supported that the protective effect of BAA depends on the regulation of intracellular calcium homeostasis.

Conclusion: BAA exerts antiepileptic effects by inhibiting neuronal calcium overload and modulating the JAK2/STAT3 signaling pathway, thereby attenuating neuroinflammation and apoptosis. These findings provide a solid experimental foundation for developing BAA as a promising antiepileptic candidate and elucidate its multi-target mechanism of action.

Keywords: β-amyrin acetate, epilepsy, calcium overload, reactive oxygen species, neuroinflammation, apoptosis

Introduction

Epilepsy is a chronic neurological disorder characterized by recurrent and unprovoked seizures. It poses a substantial global health challenge, affecting more than 70 million individuals worldwide, with rates ranging from 50.4 to 81.7 cases per 100,000 population.[1] Despite advancements in genetics and therapeutics, critical gaps persist in precise diagnosis, mechanistic understanding, and effective management.[2] Valproate (VPA), a first-line antiepileptic drug, is effective but its use is constrained by significant adverse effects, including teratogenicity, hepatotoxicity, and drug interactions.[3] Therefore, there is a pressing need to develop novel therapeutic agents with enhanced efficacy and improved safety profiles.

https://doi.org/10.2147/DDDT.S566649
Received: 24 November 2025
Accepted: 7 April 2026
Published: 20 April 2026

Traditional Chinese medicine has attracted attention for its potential to treat refractory neurological diseases, owing to its multi-target mechanisms and favorable safety profile.[4] BAA, a pentacyclic triterpenoid and acetylated derivative of β-Amyrin, is widely present in medicinal plants such as Kansui Radix, Cirsium japonicum, and Taraxacum officinale, and has been reported to exhibit potent anti-inflammatory activity.[5] Previous studies have shown that an α/β-amyrin mixture prolongs seizure latency and survival time in a PTZ-induced epileptic model, potentially by modulating the GABAergic system and protein kinase C (PKC) signaling pathway.[6] Furthermore, β-amyrin enhances antioxidant enzyme activity, ameliorates oxidative stress, and confers neuroprotection by suppressing pro-inflammatory cytokines such as interleukin-6 (IL-6), interleukin-1β (IL-1β), and tumor necrosis factor-α (TNF-α).[7,8] Compared to β-amyrin, BAA possesses lower polarity and higher lipophilicity, suggesting a greater potential to cross the BBB and exert enhanced central nervous system effects.[9,10] However, the anti-seizure effects of BAA itself and its underlying mechanisms remain entirely unexplored.

The initiation of epileptic seizures involves a disruption of the critical balance between excitatory neurotransmitters (eg, Glu, aspartate) and inhibitory neurotransmitters (eg, γ-aminobutyric acid (GABA), glycine).[11,12] PTZ, a GABA_A receptor antagonist, attenuates inhibitory, leading to neuronal hyperexcitability and synchronized discharges. This hyperexcitability triggers excessive Glu release and overactivation of N-methyl-D-aspartate (NMDA) receptors, resulting in a pathological influx of calcium ions (Ca^{2+}) and intracellular calcium overload. Calcium overload subsequently activates calcium-dependent enzymes, disrupts mitochondrial function, and promotes excessive reactive oxygen species (ROS) generation, culminating in oxidative stress, neuronal excitotoxicity.[13–15] Notably, excessive ROS can activate Janus kinase 2 (JAK2) via direct oxidation and inhibition of phosphatases, leading to its phosphorylation and subsequent recruitment and phosphorylation of downstream Signal Transducer and Activator of Transcription 3 (STAT3).[16–18] Phosphorylated STAT3 (p-STAT3) dimerizes, translocates to the nucleus, and regulates the transcription of genes involved in proliferation, survival, migration, inflammation, and anti-apoptosis. Critically, calcium overload is a pivotal driver of these downstream pathological events. However, therapeutic strategies specifically and effectively targeting this key node remain limited.

Zebrafish have emerged as a robust and genetically tractable vertebrate model for epilepsy research, owing to their conserved neuroanatomy, high-throughput suitability, reliable behavioral, and electrophysiological seizure phenotypes. Their transparent larvae and rapid drug absorption further enable efficient in vivo screening of anti-seizure compounds and mechanistic investigation.[19] The brains of zebrafish larvae share fundamental structural and functional characteristics with mammalian brains, including conserved neurotransmitter systems such as GABAergic and glutamatergic signalling, and well-defined neural circuits that underpin seizure generation.[20] The PTZ-induced seizure model in zebrafish reproduces key behavioural and electroencephalographic features of human seizures. These are characterised by a dose-dependent progression from increased movement to clonic jerks, and ultimately to tonic-clonic seizures.[21,22] Zebrafish larvae develop a fully formed nervous system within seven days post-fertilisation. Their BBB is not yet fully mature, facilitating direct access of drugs to the central nervous system via immersion. This reduces the cost and operational complexity of drug screening.[23] Therefore, this model is suitable for evaluating the efficacy of candidate antiepileptic drugs at the whole-organism level. In this study, we used a PTZ-induced zebrafish epilepsy model to evaluate the in vivo antiepileptic efficacy of BAA and assess its effects on seizure-induced oxidative stress, apoptosis, and neuroinflammation.

Our research aims to comprehensively evaluate the antiepileptic effects of BAA, investigating whether it exerts neuroprotective effects by modulating neuronal calcium overload and its downstream pathways. To evaluate the therapeutic efficacy of BAA in vivo, we established a PTZ-induced epileptic zebrafish model. Using a combination of network pharmacology and molecular docking techniques, we predicted the potential targets and related pathways of BAA. Using a Glu-induced HT-22 neuronal injury model, we validated the regulatory effects of BAA on calcium homeostasis, oxidative stress, neuroinflammation, and apoptosis at a cellular level. This study provides new insights into the development of multi-target antiepileptic drugs and establishes an experimental basis for developing BAA as an antiepileptic candidate compound.

Materials and Methods

Zebrafish Maintenance and Egg Collection

Wild-type adult zebrafish were purchased from Nanjing Yishu Lihua Co., Ltd. (China) and maintained at 28 °C under a 10 h/14 h light/dark cycle, as previously described. The fish were fed live brine shrimp three times daily. After 7 days of acclimation under laboratory conditions, zebrafish were segregated into spawning tanks at a 2:1 male-to-female ratio. Embryos were collected 2 h after segregation, and all experiments were conducted using zebrafish larvae at 7 days post-fertilization (dpf).

Zebrafish Experimental Design

Different treatments were applied to zebrafish larvae to study the effect of BAA (TargetMol, Cat#TN1438) on PTZ (Aladdin, Cat#P103065) induced seizures.[24] Before the experiment, zebrafish larvae were randomly assigned to each treatment group, with 12 fish per group. The room temperature was maintained at 28°C, and five independent experiments were conducted. The experimental design consists of four treatment groups, outlined as follows:

Control group: Larvae in this group received no additional compounds.

PTZ group: Larvae in this group were exposed to 10 mM PTZ for 30 min at 7 dpf to induce seizures and establish the pathological state.

PTZ + VPA (1 mM) group: Larvae in this group were pre-treated with 1 mM VPA for 12 h at 6 dpf, and then exposed to 10 mM PTZ for 30 min at 7 dpf.

PTZ + BAA (2.5 μM / 10 μM) group: Larvae in this group were pre-treated with 2.5 μM/10 μM BAA for 12 h at 6 dpf, and then exposed to 10 mM PTZ for 30 min at 7 dpf.

Zebrafish Behavioral Analysis

To assess the effects of BAA on PTZ-induced locomotor deficits, we measured swimming behavior parameters in zebrafish larvae, including total distance traveled and average speed. Zebrafish larvae at 6 dpf were treated with 2.5 μM / 10 μM BAA and 1 mM VPA for 12 h. At 7 dpf, the larvae were exposed to 10 mM PTZ. Immediately following PTZ exposure, behavioral analysis was performed for 30 min using an automated Zebrafish Behavioral Analysis System (Hunter Lab, HT-XW2D-2100). In the trajectory plots, the line density corresponds to the total distance traveled by zebrafish within 30 min. Based on swimming speed, seizure-like behaviors in zebrafish were classified into three distinct stages: Stage I: Increased Activity - After initial drug administration, the overall activity level of zebrafish increased, but the swimming pattern remained normal. Black lines represent low-speed movement (speed < 20 mm/s). Stage II: Clonic Seizures - Zebrafish exhibited brief, rapid jerks or "darting" movements with uncoordinated swimming. Green lines represent medium-speed movement (speed: 20 mm/s - 50 mm/s). Stage III: Tonic-Clonic Seizures - Characterized by typical "racing" behavior, where zebrafish lost balance and displayed extremely high-speed, uncontrolled bursts of movement along the tank edge or in a single direction, often in circles. This phase is a core evaluation indicator in the PTZ model. Red lines represent high-speed movement (speed > 50 mm/s).

Zebrafish Acridine Orange (AO) Staining and ROS Staining

DCFH-DA (Aladdin, Cat# H131224) is a fluorescent probe used for detecting ROS, while Acridine Orange (AO) (Aladdin, Cat# A100495) staining reflects apoptosis. Zebrafish larvae from both Control and treatment groups were immersed in solutions containing 5 μg/mL AO and 20 μg/mL DCFH-DA, respectively, and incubated in the dark at room temperature for 30 min. After washing, the larvae were anesthetized using a 0.02% tricaine solution (Aladdin, Cat#E107465). Fluorescence in each group of zebrafish larvae was observed and imaged using a zebrafish imaging system (Hunter Lab, HT-CX-001) (excitation at 488 nm and emission at 525 nm), and the images were analyzed with ImageJ.

Target Screening

Potential human targets of BAA were predicted using the Swiss Target Prediction platform (http://www.swisstargetprediction.ch/), the Pharm Mapper database (http://lilab-ecust.cn/pharmmapper/), the Integrated Pharmacology-based

Traditional Chinese Medicine Research Platform (http://www.tcmip.cn/), and the Drug Bank database (https://go.drugbank.com/). Duplicate targets were removed, and the remaining targets were standardized and unified using the UniProt database to obtain the target set of the active ingredient BAA. Disease-related targets for epilepsy were retrieved from the TTD database (https://db.idrblab.net/ttd/) and the Gene Cards database (https://www.genecards.org/) using "epilepsy" as the search term. After removing duplicates, the remaining targets were also standardized via UniProt to obtain epilepsy-associated targets. Both the BAA target set and the epilepsy target set were imported into the bioinformatics online platform (https://www.bioinformatics.com.cn/) to generate a Venn diagram and extract information on overlapping targets between BAA and epilepsy. A PPI network was constructed using the STRING database (confidence score > 0.7) and visualized with Cytoscape 3.9.1. Core targets were screened based on topological features (degree, betweenness centrality, closeness centrality). Gene Ontology (GO) and Kyoto Encyclopedia of Genes and Genomes (KEGG) enrichment analyses were performed using DAVID (v6.8) with a significance threshold of FDR < 0.05.

Molecular Docking

The protein's secondary structure was downloaded in PDB format from the Protein Data Bank (https://www.rcsb.org/). The protein structure was processed using AutoDock Tools 1.5.6 to remove water molecules, add charges, and add hydrogen atoms. The structure of the active component BAA was downloaded and saved from the Traditional Chinese Medicine Systems Pharmacology Database and Analysis Platform (TCMSP, http://tcmspw.com/tcmsp.php), and the resulting structure was converted to PDB format. Molecular docking was performed using AutoDock Tools 1.5.6 to calculate binding energy. The results were imported into PyMOL software for visual display of the docking outcomes.

Cell Culture

The HT-22 neuronal cell line was obtained from Shanghai Zhong Qiao Xin Zhou Biotechnology Co., Ltd. (China). HT-22 cells were cultured in DMEM supplemented with 10% FBS, penicillin, and streptomycin. All cell lines were authenticated by quantitative PCR (qPCR) or Western Blot, and tested negative for mycoplasma contamination.

Cell Viability Assay

The CCK-8 assay kit (Linbio, Cat#LC300105) was used to measure cells viability. HT-22 neuronal cell were seeded in 96-well plates at a density of 1×10^4 cells per well. The cells were treated with Glu (2.5, 5, 10, 20, 40 μM) or BAPTA-AM (0.125, 0.25, 0.5, 1, 5, 10 μM) or Glu (20 mM) + BAA (2.5, 5, 10, 20 μM) or Glu (20 mM) + BAPTA-AM (0.25 μM) or Glu (20 mM) + BAPTA-AM (0.25 μM) + BAA (10 μM) for 24 h. Then, 10 μL of CCK-8 solution was added to each well, followed by incubation for 2 h. The optical density (OD) was measured at 450 nm using a microplate reader (MD, SpectraMax ID5). All experiments were performed in 96-well plates with six biological replicates.

Annexin V/PI Double Staining for Apoptosis Detection

The Annexin V/PI Apoptosis Detection Kit (Linbio, Cat#LC300303) was used to assess cell apoptosis. HT-22 cells in logarithmic growth phase were seeded at a density of 3×10^5 cells per well in 6-well plates. The cells were then co-treated with 20 mM Glu and 2.5 or 10 μM BAA or 0.25 μM BAPTA-AM or BAPTA-AM (0.25 μM) + BAA (10 μM) 24 h. Apoptosis was measured using a flow cytometer (Beamdiag, Beam Cyte-1026). Annexin V-FITC: Excited at 488 nm, detected in the 530 nm channel; PI: Excited at 488 nm, detected in the 585 nm channel.

Measurement of Intracellular ROS and Calcium Expression

The Fluo-4 AM fluorescent dye (Beyotime, Cat#S1060) was used to detect intracellular calcium levels. HT-22 cells were seeded in 96-well plates at a density of 1×10^4 cells per well and co-treated with 20 mM Glu and 2.5 or 10 μM BAA for 24 h at 37 °C. Then, 100 μL of DCFH-DA (20 μg/mL) or Fluo-4 AM (2 μM) was added to each well. After incubation, the cells were washed twice with PBS. Fluorescence and bright-field images were captured using a Zeiss fluorescence microscope (excitation at 488 nm and emission at 525 nm) and analyzed with ImageJ.

qPCR Analysis and Primer Sequences

Total RNA was isolated from zebrafish larvae and cell samples using the TRIzol® Reagent Extraction Kit (Vazyme, Cat#R401-01-AA) according to the manufacturer's instructions. The extracted RNA was used as a template to synthesize cDNA with a Reverse Transcription Kit (Sparkjade, Cat#AG0304) in a gradient PCR instrument (Bio-Rad, T100). Gene-specific primers were synthesized by Sangon Biotech Co., Ltd. Amplification was performed using SYBR Green qPCR Mix (Sparkjade, Cat#AH0101) on a qPCR system (Applied Biosystems 7500). The thermal cycling conditions were as follows: 50 °C for 2 min, 95 °C for 3 min, followed by 40 cycles of 94 °C for 15s and 60 °C for 1 min. The relative mRNA expression levels of target genes were calculated using the 2-ΔΔCt method with *β-actin* as the internal reference gene. The corresponding forward and reverse primers used for qPCR analysis are listed in Supplementary Table S1.

Western Blot Analysis and Antibodies

Cell samples were lysed on ice for 20 min using RIPA lysis buffer containing protease and phosphatase inhibitors. The lysates were then centrifuged at 12000 rpm for 10 min to obtain clear supernatants. Subsequently, the cell lysates were heated at 100 °C for 5–8 min. The proteins were separated by SDS-PAGE and transferred onto a nitrocellulose membrane (Millipore, Cat#HATF00010). After blocking with 5% skim milk for 1 h at room temperature, the membrane was incubated with primary antibodies overnight at 4 °C, followed by incubation with secondary antibodies for 1 h at room temperature. Super-sensitive chemiluminescence reagent (Sparkjade, Cat#ED0016) was applied to the blot, and images were captured using a gel imaging system (BIO-RAD, ChemiDoc MP Imaging System). The following antibodies were used: IL-6 (Zenbio, Cat#500286, 1:1000), STAT3 (Abcam, Cat#ab68153, 1:1000), phospho-STAT3 (Y705) (Abcam, Cat#ab267373, 1:1000), JAK2 (Zenbio, Cat#R24775, 1:1000), phospho-JAK2 (Tyr1007/1008) (Zenbio, Cat#R381556, 1:1000), Caspase3 (proteintech, Cat#66470-2-Ig, 1:1000), Cleaved caspase-3 (Zenbio, Cat#341034, 1:1000), Bax (CST, Cat#2772T, 1:1000), Bcl-2 (Abcam, Cat#ab182858, 1:1000), β-actin (proteintech, Cat#81115-1-RR, 1:3000) See Appendix for original uncropped blots.

Statistics Analysis

Statistical analysis was performed using GraphPad Prism software. All data are presented as mean ± SEM. Normality was assessed using the Shapiro–Wilk test, and homogeneity of variance was evaluated using Levene's test. For comparisons among multiple groups, one-way ANOVA followed by Tukey's post hoc test was applied. For comparisons between two groups, a two-tailed Student's *t*-test was used. A p-value < 0.05 was considered statistically significant. All experiments were repeated at least five times as independent biological replicates.

Results

Inhibitory Effect of BAA on PTZ-Induced Epileptiform Locomotion in Zebrafish Larvae

Except for the Control group, zebrafish larvae in all other groups were treated with PTZ at 7 dpf for 30 min to establish a PTZ-induced epilepsy model. The interventional effect of BAA on PTZ-induced epileptic-like movements in zebrafish larvae was evaluated through behavioral analysis. Zebrafish larvae treated with 2.5, 5, 10, and 20 μM BAA showed no obvious mortality or morphological abnormalities (Supplementary Figure S1). Compared to the Control group, the PTZ group exhibited intensive, crossing, and non-directional darting movements (Figure 1A). Within 0–15 min of PTZ treatment, swimming speed rapidly increased from baseline (1.2 ± 0.2 mm/s) to a peak (5.5 ± 0.2 mm/s), which was 4.58 times higher than that of the Control group during the same period. After 30 min of treatment, the speed stabilized at 4.3 ± 0.2 mm/s (p < 0.0001 vs Control group)(Figure 1B). Meanwhile, the total swimming distance of the PTZ group over 30 min increased significantly to 9073 ± 230.8 mm, representing a 394% increase compared to the Control group (1835 ± 199.2 mm, p < 0.0001 vs Control group)(Figure 1C). The total distance of clonic seizures increased to 3053 ± 119 mm (p < 0.0001 vs Control group)(Figure 1D), and the total distance of tonic-clonic seizures increased to 2040 ± 90 mm (p < 0.0001 vs Control group)(Figure 1E). The results showed that PTZ treatment significantly increased motor activity and induced Phase II clonic seizures and Phase III tonic-clonic seizures, indicating the successful establishment of the epilepsy model.

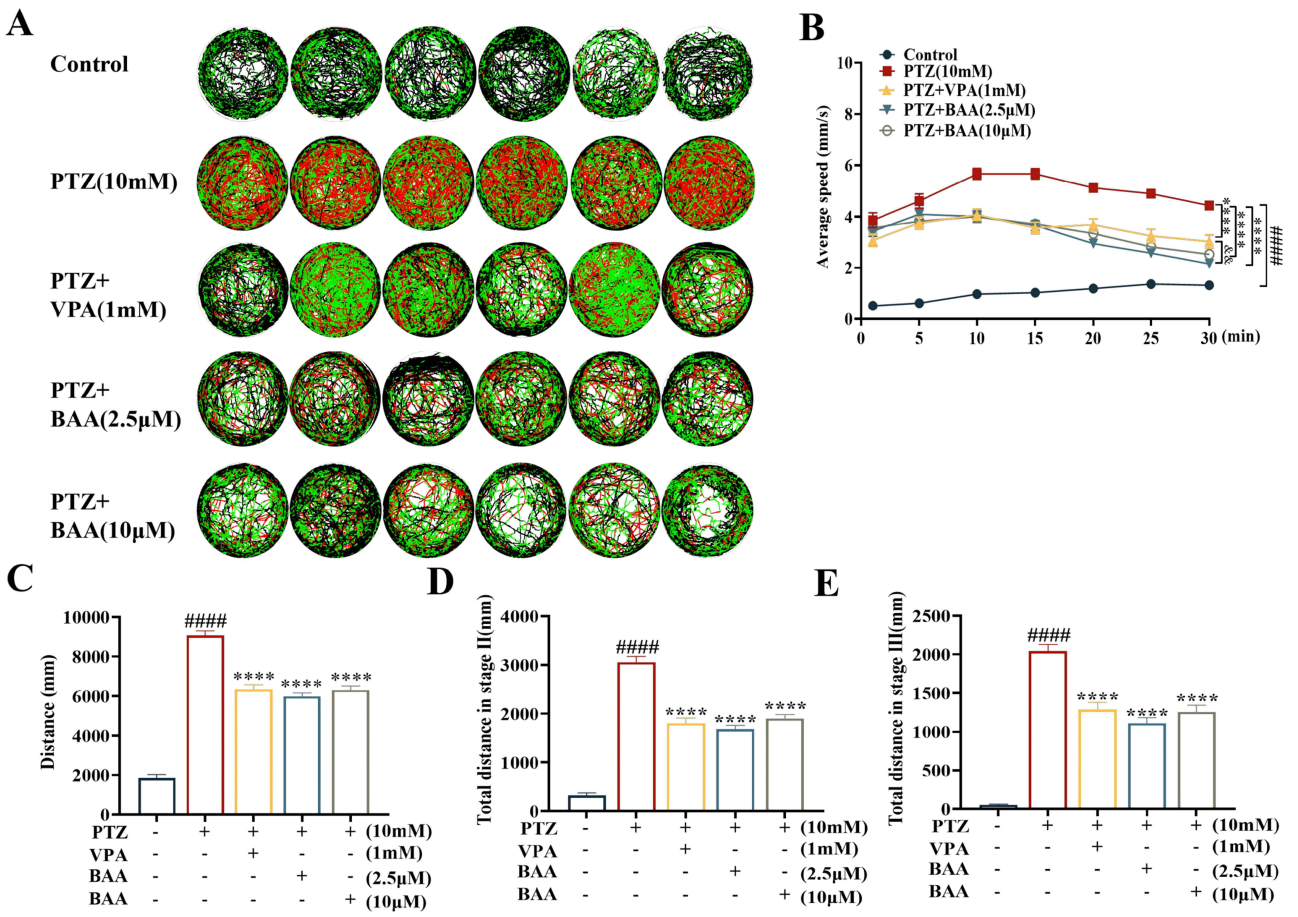

Figure 1 BAA pretreatment attenuates PTZ-induced epileptiform locomotor activity in 7 dpf zebrafish larvae (**A**) Movement trajectories; (**B**) Mean swimming velocity; (**C**) Total swimming distance; (**D**) Total distance during Stage II seizures; (**E**) Total distance during Stage III seizures. Larvae at 6 dpf were pretreated with 1mM VPA, 2.5 μM BAA, or 10 μM BAA for 12 h, and then exposed to 10 mM PTZ at 7 dpf. Locomotor activity was recorded for 30 min using a behavioral analysis system. Red trajectories indicate high-speed movement (> 50mm/s, corresponding to Stage III seizures); green trajectories indicate medium-speed movement (20–50 mm/s, corresponding to Stage II seizures); black trajectories indicate low-speed movement or stationary behavior (< 20mm/s). Data are presented as mean ± SEM. n = 60 larvae per group from 5 independent biological replicates (12 larvae per replicate). $^{\#\#\#\#}p < 0.001$ vs Control group; $^{****}p < 0.001$ vs PTZ group; $^{\&\&}p < 0.01$ vs VPA group.

Compared to the PTZ group, both the VPA and BAA treatment groups exhibited suppressed hyperexcitability, as evidenced by reduced swimming speed over 30 min (VPA group: 3.1 ± 0.3 mm/s; 2.5 μM BAA group: 2.2 ± 0.1 mm/s; 10 μM BAA group: 2.5 ± 0.2 mm/s; all $p < 0.0001$ vs PTZ group) and significantly decreased total movement distance (VPA group: 6345 ± 238.3 mm; 2.5 μM BAA group: 5988 ± 172.7 mm; 10 μM BAA group: 6314 ± 200.6 mm; all $p < 0.0001$ vs PTZ group). The distances of clonic seizures (VPA group: 1805 ± 108.2 mm; 2.5 μM BAA group: 1686 ± 75.3 mm; 10 μM BAA group: 1902 ± 79.1 mm) and tonic-clonic seizures (VPA group: 1287 ± 92.3 mm; 2.5 μM BAA group: 1110 ± 70.6 mm; 10 μM BAA group: 1256 ± 85.4 mm) were also significantly reduced (all $p < 0.0001$ vs PTZ group). Notably, 2.5 μM BAA had a more significant effect on reducing swimming speed than VPA ($p = 0.004$ vsVPA group). In the zebrafish model, the median effective dose (ED_{50}) of VPA was reported as 198.7 mg/kg (approximately 1 mM).[25] In contrast, BAA exhibited antiepileptic effects at a concentration of 2.5 μM (approximately 0.73 mg/kg), corresponding to an approximately 73-fold higher potency on a molar basis. These results suggest that BAA may have stronger antiepileptic activity than VPA in this model.

BAA Alleviates PTZ-Induced Oxidative Stress and Apoptosis in Zebrafish Larvae

Oxidative stress arises from an imbalance between the generation of free radicals and the antioxidant defense system.[26] During epileptic seizures, neuronal hyperactivity can lead to excessive production of free radicals, thereby inducing oxidative stress and causing neuronal damage.[27] To evaluate the levels of ROS in zebrafish, this study employed DCFH-DA staining to detect ROS in 7 dpf larvae. The results showed that the ROS fluorescence intensity in the PTZ group (1.2

± 0.1) was significantly increased by approximately 6-fold compared to the Control group (0.2 ± 0.1) ($p < 0.0001$ vs Control group). In contrast, BAA pretreatment markedly reversed the PTZ-induced increase in ROS (2.5 μM BAA group: 0.3 ± 0.1; 10 μM BAA group: 0.3 ± 0.1; both $p < 0.0001$ vs PTZ group), restoring it to a level comparable to that of the Control group (Figure 2A and B).

Excessive ROS can disrupt mitochondrial membrane integrity, promoting the release of pro-apoptotic factors, such as cytochrome c, into the cytoplasm, which subsequently activates Caspase-9 and its downstream effector, Caspase-3, ultimately initiating the intrinsic apoptotic pathway.[28] Consistent with the reduction in ROS levels, AO staining revealed that the AO fluorescence intensity in the PTZ group (5.9 ± 0.2) was significantly increased by approximately 1.9-fold compared to the Control group (3.1 ± 0.4) ($p < 0.0001$ vs Control group). Moreover, BAA pretreatment significantly suppressed the PTZ-induced increase in AO fluorescence intensity (2.5 μM BAA group: 3.3 ± 0.1; 10 μM BAA group: 2.6 ± 0.1; both $p < 0.0001$ vs PTZ group), restoring it to a level comparable to that of the Control group (Figure 2C and D). These results suggest that BAA may confer neuroprotective effects by alleviating PTZ-induced oxidative stress and subsequent apoptosis.

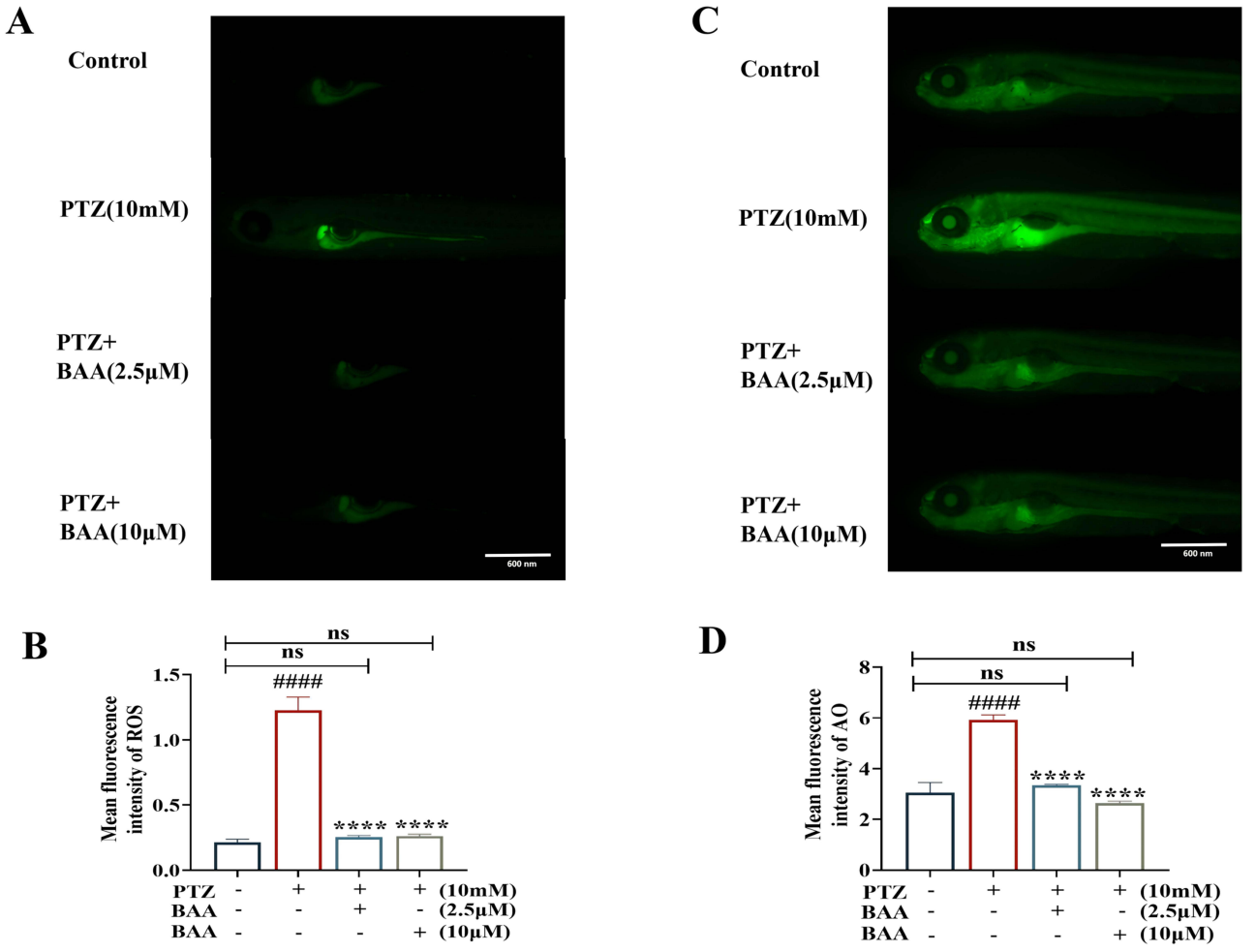

Figure 2 BAA alleviates PTZ-induced oxidative stress and cell death in 7 dpf zebrafish larvae. (**A**) ROS staining (DCFH-DA) images; (**B**) Quantification of ROS fluorescence intensity; (**C**) Apoptosis staining (AO) images; (**D**) Quantification of AO fluorescence intensity. 6 dpf larvae were pretreated with 1 mM VPA, 2.5 μM BAA, or 10 μM BAA for 12 h. At 7 dpf, they were exposed to 10 mM PTZ for 30 min and then stained with 20 μg/mL DCFH-DA or 5 μg/mL AO for 20 min. Fluorescence images were captured using a zebrafish imaging system (4× objective magnification). Data are presented as mean ± SEM. n = 30 larvae per group from 5 independent biological replicates (6 larvae per replicate). $^{\#\#\#\#}p < 0.0001$ vs Control group; $^{****}p < 0.0001$ vs PTZ group.
Abbreviation: ns, no significant difference.

https://doi.org/10.2147/DDDT.S566649

BAA Attenuates PTZ-Induced Neuronal Hyperexcitation and Neuroinflammation to Exert Antiepileptic Effects in Zebrafish

PTZ induces neuronal hyperexcitability by inhibiting GABAergic transmission, whereas enhancing GABAergic signaling reduces neuronal excitability and suppresses c-fos expression.[29] As a classical marker of enhanced neuronal electrical activity, c-fos expression can be rapidly induced within a short period by the synchronized high-frequency discharges of neurons during epileptic seizures.[30] The expression level of *c-Fos* mRNA in zebrafish larvae treated with PTZ for 30 min (3.9 ± 0.4) was significantly increased by 3.9-fold compared to the Control group (1.0 ± 0.1) ($p < 0.0001$vs Control group). Pretreatment with BAA significantly inhibited the PTZ-induced upregulation of *c-Fos* expression, restoring it to near-normal levels (2.5 μM BAA: 1.1 ± 0.1; 10 μM BAA: 1.8 ± 0.3; both $p < 0.0001$ vs PTZ group), suggesting that BAA effectively alleviates neuronal hyperexcitation (Figure 3A).

Neuronal hyperexcitation not only causes neuronal damage but also triggers an inflammatory cascade. After seizures, the upregulated expression of pro-inflammatory cytokines (such as *Il-1β, Il-6, Tnf-α*, etc.) may exacerbate neuronal injury and promote epileptic recurrence.[31] To evaluate the regulatory effect of BAA on neuroinflammation, this study measured the mRNA levels of inflammatory factors in 7 dpf zebrafish larvae using qPCR. PTZ treatment significantly increased the expression of pro-inflammatory factors: compared to the Control group, the mRNA expression of *Tnf-α* was upregulated by 2.4-fold ($p < 0.0001$ vs Control group), *Il-6* by 2.2-fold ($p = 0.03$ vs Control group), *Il-1β* by 6.2-fold ($p = 0.0005$ vs Control group), and *Cox-2* by 2.1-fold ($p = 0.015$ vs Control group) in the PTZ group. In contrast, pretreatment with 10μM BAA significantly suppressed the PTZ-induced upregulation of these factors, *Tnf-α* ($p = 0.0012$ vs PTZ group), *Il-1β* ($p = 0.0076$ vs PTZ group), *Il-6* ($p = 0.0396$ vs PTZ group), and *Cox-2* ($p = 0.2031$ vs PTZ group), restoring their expression to levels comparable to those of the Control group (Figure 3B–E). These results indicate that BAA can inhibit PTZ-induced neuronal hyperexcitation and neuroinflammatory.

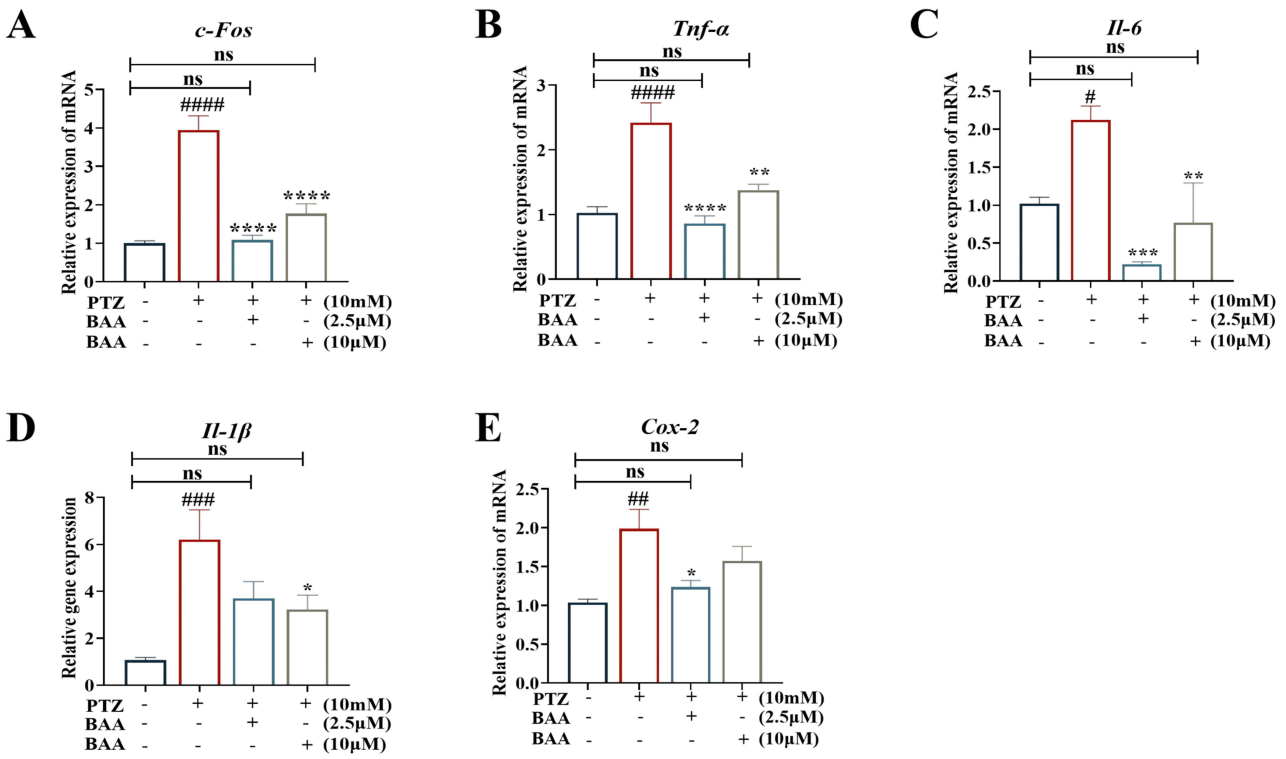

Figure 3 BAA inhibits PTZ-induced excitability and expression of inflammatory markers in zebrafish larvae. (**A**) *c-Fos*, (**B**) *Tnf-α*, (**C**) *Il-6*, (**D**) *Il-1β*, (**E**) *Cox-2* mRNA expression levels. Zebrafish larvae at 6 dpf were pretreated with 2.5 μM BAA or 10 μM BAA for 12 h, and larvae at 7 dpf were treated with 10 mM PTZ for 30 min. *β-actin* was used as the internal reference. Data are presented as mean ± SEM. n = 60 larvae per group from 5 independent biological replicates (12 larvae per replicate). $^{\#}p < 0.05$, $^{\#\#}p < 0.01$, $^{\#\#\#\#}p < 0.001$, $^{\#\#\#\#\#}p < 0.001$ vs Control group; $^{*}p < 0.05$, $^{**}p < 0.01$, $^{***}p < 0.001$, $^{****}p < 0.0001$ vs PTZ group.

Abbreviation: ns, no significant difference.

https://doi.org/10.2147/DDDT.S566649

Network Pharmacology and Molecular Docking Reveal the Anti-Epileptic Mechanism of BAA

To further elucidate the molecular mechanisms underlying the anti-epileptic effects of BAA, network pharmacology and molecular docking were employed to identify potential targets. A total of 110 drug targets of BAA were retrieved from four databases, and 9640 epilepsy-related genes were collected from two databases. After intersection, 91 potential targets for BAA in the treatment of epilepsy were identified (Figure 4A). A PPI network was constructed from these 91 targets, in which JAK2 and Bcl-2 exhibited high network centrality (Figure 4B). GO functional analysis yielded 412 biological processes, and KEGG pathway analysis identified 68 signaling pathways. KEGG enrichment analysis revealed that the intersecting targets were significantly enriched in the calcium signaling pathway, HIF-1 signaling pathway, and VEGF signaling pathway, among others (Figure 4C and D). Molecular docking was performed to evaluate the binding affinity between BAA and the key targets Bcl-2 and JAK2. The results demonstrated strong binding interactions, with binding energies of −13.38 kcal/mol for Bcl-2 and −11.84 kcal/mol for JAK2 (Figure 4E).

BAA Attenuates Oxidative Stress by Stabilizing Calcium Homeostasis and Disrupting the "ROS-Ca^{2+}" Positive Feedback Loop

Based on network pharmacology predictions, BAA may regulate calcium signaling pathways. To validate this hypothesis, we used a Glu-induced HT-22 cell injury model. The CCK-8 assay showed that Glu exhibited significant concentration-dependent toxicity toward HT-22 cells, with an IC_{50} value of 26.11 mM (Figure 5A). Considering model stability and cell

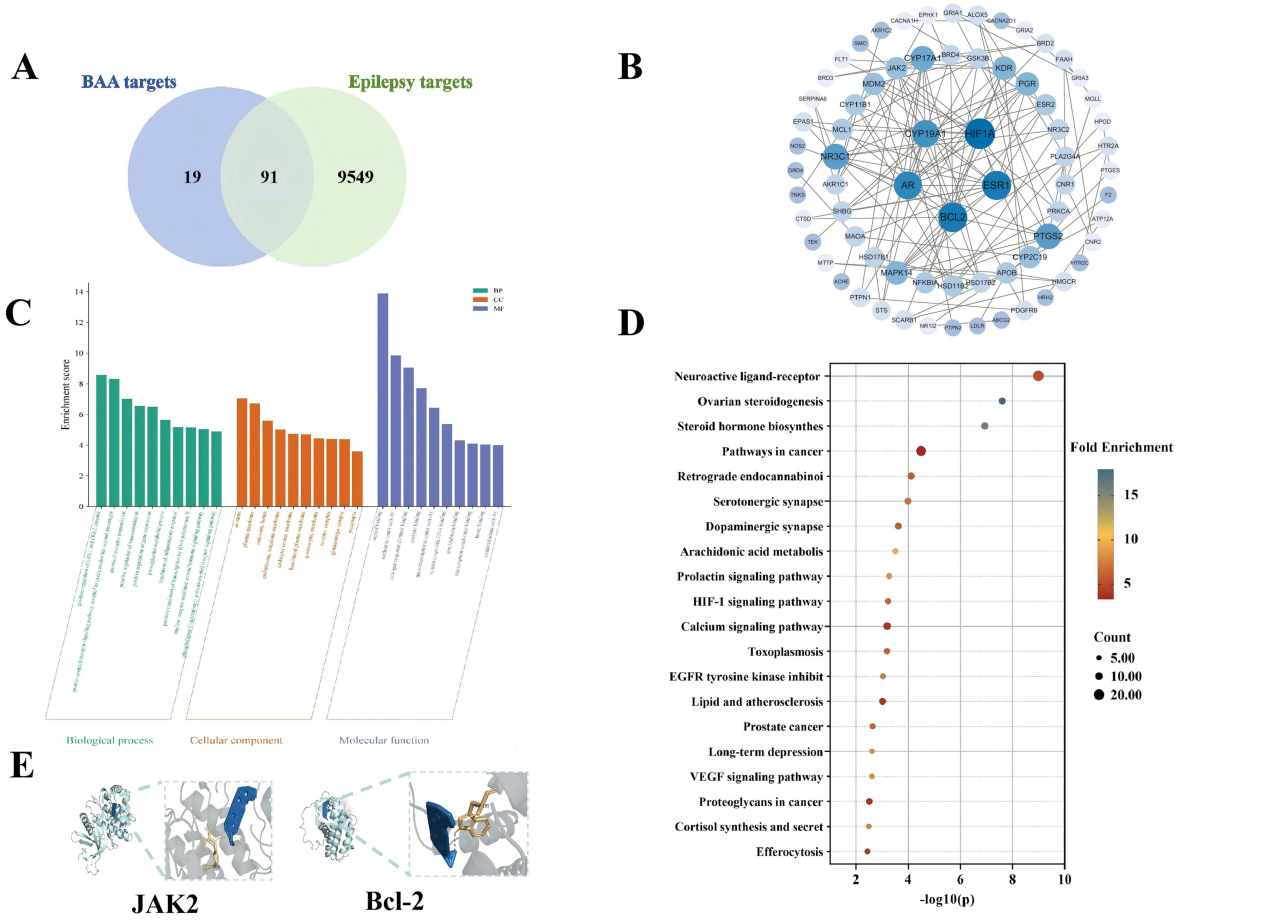

Figure 4 Network pharmacology and molecular docking of BAA and epilepsy. (**A**) Venn diagram of drug and disease intersection targets; (**B**) PPI network diagram of BAA-epilepsy intersection targets; (**C**) GO (BP, CC, MF) triad diagram; (**D**) KEGG enrichment bubble diagram; (**E**) Molecular docking binding energy between BAA and JAK2: −11.84 kcal/mol; Molecular docking between BAA and Bcl-2, with a binding energy of −13.38 kcal/mol.

https://doi.org/10.2147/DDDT.S566649

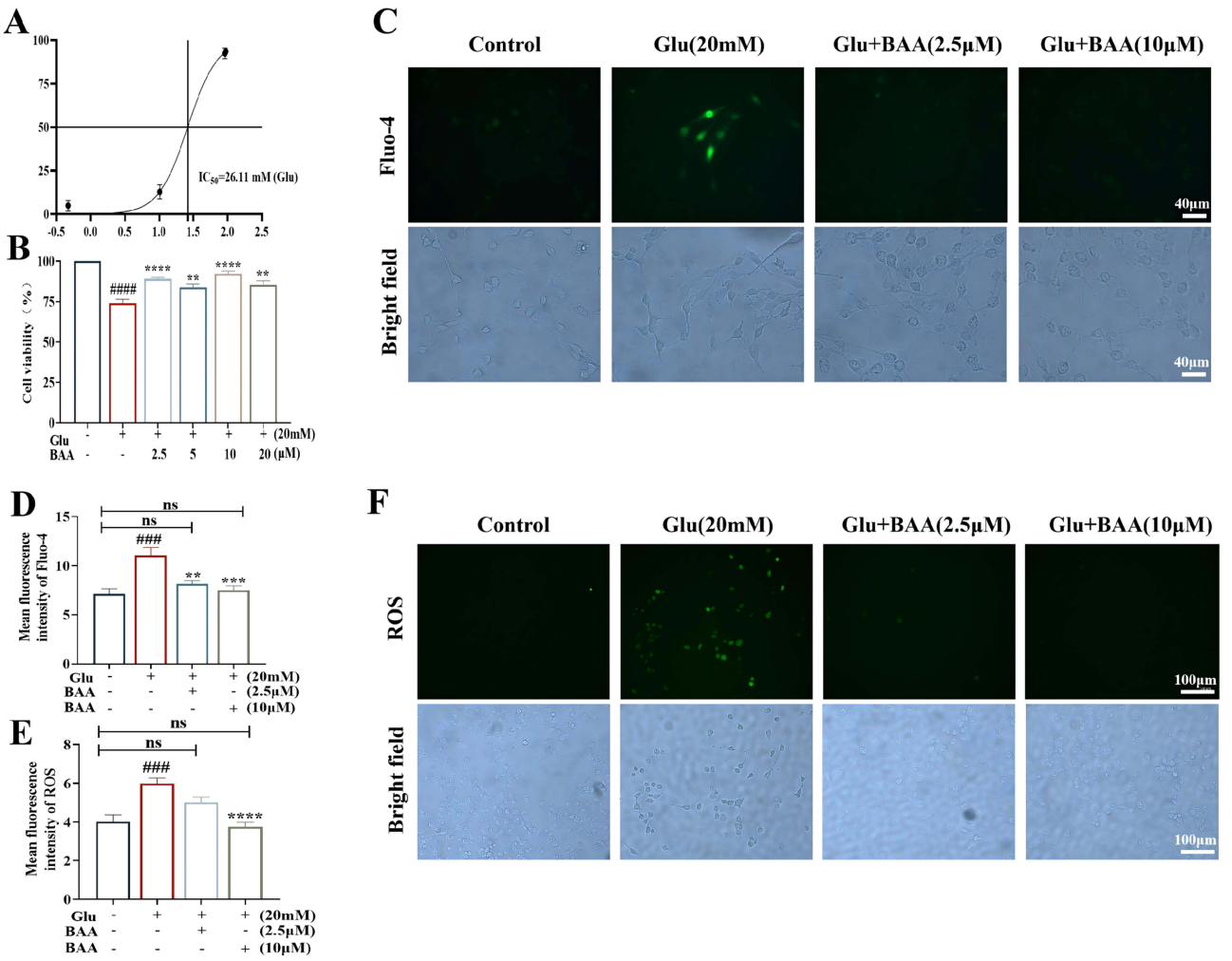

Figure 5 BAA alleviates Glu-induced cytotoxicity, calcium overload, and oxidative stress in HT-22 cells. (**A**) The CCK-8 assay was used to evaluate the effects of different concentrations of Glu (2.5, 5, 10, 20, and 40 mM) on the viability of HT-22 cells after 24 h of treatment, and the half-maximal inhibitory concentration (IC_{50}) was calculated; (**B**) BAA reverses the Glu-induced decrease in HT-22 cells' viability. The CCK-8 assay was used to evaluate the effects of different concentrations of BAA (2.5, 5, 10, 20 μM) on the viability of HT-22 cells treated with 20 mM Glu for 24 h; (**C**) BAA inhibits Glu-induced increase in intracellular Ca^{2+} levels in HT-22 cells. Fluorescence microscopy images of Fluo-4 staining (scale bar: 40 μm, 40x). Green: calcium signal; (**D**) Quantitative analysis of Fluo-4 fluorescence intensity; (**E**) Quantitative analysis of ROS levels; (**F**) BAA reduces Glu-induced intracellular ROS levels in HT-22 cells. Fluorescence microscopy images of ROS staining (scale bar: 50 μm, 20x). Green: DCF signal. Data are presented as mean ± SEM. n = 6 independent biological replicates per group. $^{###}p < 0.001$, $^{####}p < 0.0001$ vs Control group; $^{**}p < 0.01$, $^{***}p < 0.001$, $^{****}p < 0.001$ vs Glu group.
Abbreviation: ns, no significant difference.

condition, 20 mM Glu was selected as the inducing concentration for subsequent experiments. Consistent with the zebrafish results, 20 mM Glu stimulation for 24 h significantly induced cytotoxicity in HT-22 cells ($p < 0.0001$ vs Control group), while 2.5 μM and 10 μM BAA markedly reversed this effect, restoring cell viability to 89.0 ± 2.5% and 92.2 ± 4.0% of the Control group, respectively (both $p < 0.0001$ vs Glu group) (Figure 5B). Cells treated with 2.5 μM and 10 μM BAA exhibited normal morphology, with no obvious signs of cytotoxicity such as shrinkage, floating, or cell death (Supplementary Figure S2).

Furthermore, 20 mM Glu significantly induced ROS accumulation (DCF fluorescence intensity: 1.9-fold vs Control group, $p = 0.0003$) and cytosolic Ca^{2+} overload (Fluo-4 fluorescence intensity: 2.1-fold vs Control group, $p = 0.0004$) in HT-22 cells. Treatment with 10 μM BAA effectively reversed these effects, reducing ROS and Ca^{2+} levels to values comparable to those of the Control group (ROS: $p < 0.0001$; Fluo-4: $p = 0.0009$ vs Glu group) (Figure 5C–F). These findings suggest that BAA may effectively disrupt the "ROS–Ca^{2+}" positive feedback loop by inhibiting calcium overload, a key mechanism that amplifies oxidative stress and calcium dysregulation.

BAA Inhibits Glu-Induced Mitochondrial Apoptosis by Regulating the Bax/Bcl-2/Caspase-3 Pathway

Having demonstrated that BAA alleviates oxidative stress and calcium overload, we further investigated whether it could inhibit the downstream mitochondrial apoptotic pathway. A Glu-induced HT-22 cell apoptosis model characterized by calcium overload was established, and the apoptosis rate was assessed using flow cytometry. Additionally, Western blot analysis was performed to examine the expression of proteins such as Bax, Bcl-2, Caspase-3, and Cleaved caspase-3, aiming to elucidate the molecular mechanism by which BAA intervenes in the calcium overload-mitochondrial apoptosis pathway.

Flow cytometry results showed that after 24 h of treatment with 2.5 and 10 μM BAA, Glu-induced apoptosis was significantly inhibited ($p < 0.0001$ vs Control group), with the total apoptosis rate decreasing: from 27.2 ± 1.3% in the Glu group to 18.6 ± 1.2% in the 2.5 μM BAA group and 17.8 ± 1.0% in the 10 μM BAA group (all $p < 0.0001$ vs Glu group) (Figure 6A and B).

Western blot analysis showed that 20 mM Glu treatment for 24 h successfully activated the apoptotic execution program, as evidenced by a 1.7-fold increase in the Bax/Bcl-2 ratio ($p = 0.0051$ vs Control group) and a significant 2.1-fold increase in the Cleaved caspase-3/Caspase-3 ratio ($p = 0.0284$ vs Control group), both compared to the Control group (Figure 6C–F). Notably, pretreatment with BAA effectively reversed these effects, reducing both ratios to levels

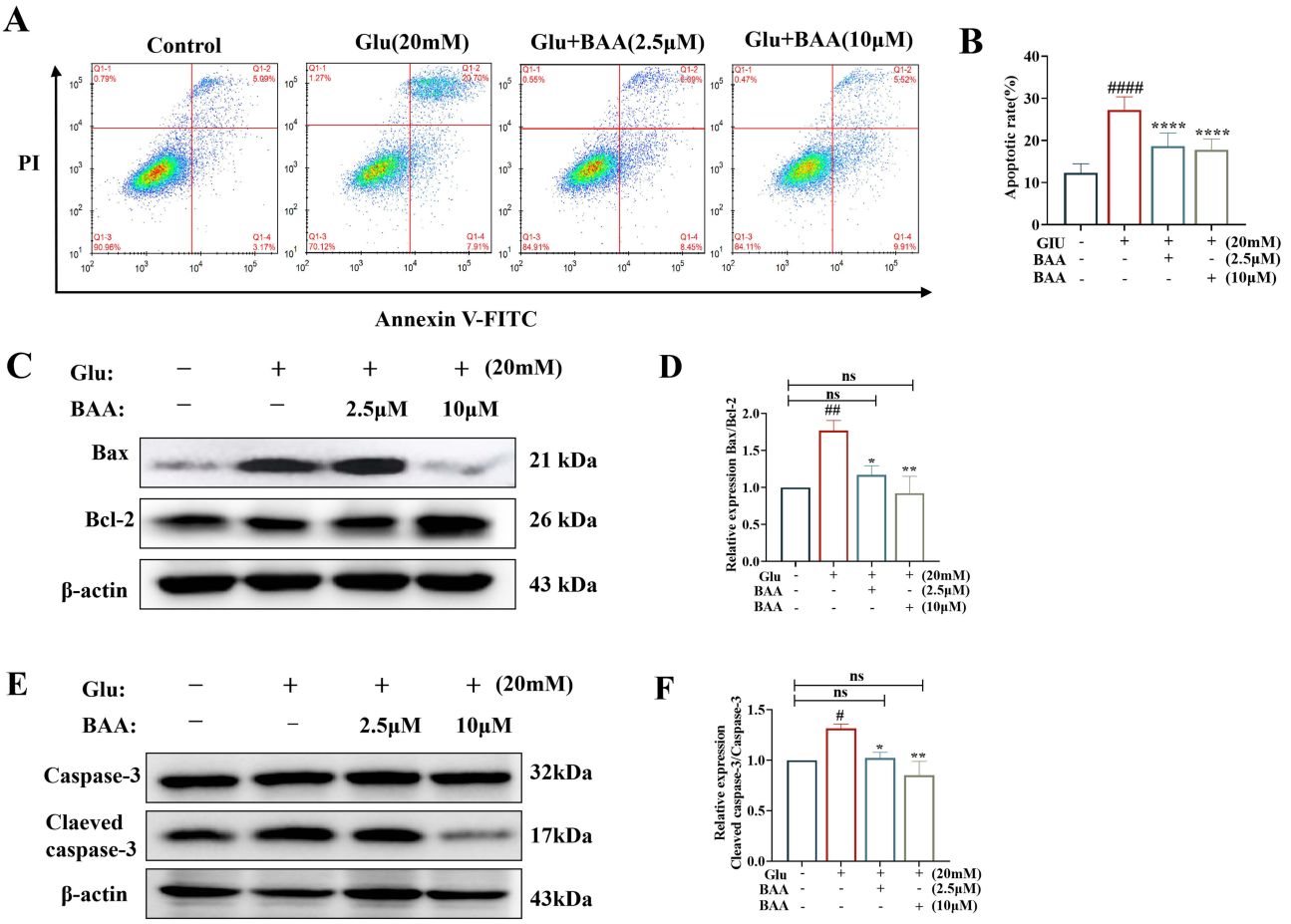

Figure 6 BAA inhibits Glu-induced apoptosis in HT-22 cells. HT-22 cells were treated with Glu (20 mM) alone or in combination with BAA (2.5, 10 μM) for 24 h. (**A**) Flow cytometry analysis with Annexin V-FITC/PI double staining was used to evaluate the effect of 2.5 and 10 μM BAA on Glu-induced apoptosis. Quadrant definitions: Q1: Necrotic cells (Annexin V^-/PI^+); Q2: Late apoptotic cells (Annexin V^+/PI^+); Q3: Viable cells (Annexin V^-/PI^-); Q4: Early apoptotic cells (Annexin V^+/PI^-); (**B**) Quantitative analysis of total apoptosis rate (Q2 + Q4). n = 6 independent biological replicates. (**C**) Western Blot bands of Bax and Bcl-2 proteins; (**D**) Quantification of Bax/Bcl-2 ratio; (**E**) Western Blot bands of Caspase-3 and Cleaved caspase-3 proteins; (**F**) Quantification of Cleaved caspase-3/Caspase-3 ratio. n = 5 independent biological replicates. β-actin was used as the loading control. Data are presented as mean ± SEM. $^{\#}p < 0.05$, $^{\#\#}p < 0.001$, $^{\#\#\#\#}p < 0.0001$ vs Control group; $^{*}p < 0.05$,$^{**}p < 0.01$, $^{****}p < 0.0001$ vs Glu group.
Abbreviation: ns, no significant difference.

https://doi.org/10.2147/DDDT.S566649

not statistically different from those of the Control group (Bax/Bcl-2 ratio: $p = 0.0271$ (2.5 μM BAA), $p = 0.0023$ (10 μM BAA); Cleaved caspase-3/Caspase-3 ratio: $p = 0.0435$ (2.5 μM BAA), $p = 0.0017$ (10 μM BAA) vs Glu group). In summary, BAA significantly rescues Glu-induced HT-22 cell apoptosis by suppressing the Bax/Bcl-2 ratio and inhibiting Caspase-3 activation, a key executioner of the mitochondrial apoptotic pathway.

BAA Alleviates Neuroinflammation by Inhibiting JAK2/STAT3 Phosphorylation and Downstream Inflammatory Factor Expression

Following the establishment of BAA's anti-apoptotic effects, we next explored its role in mitigating neuroinflammation. Given that calcium overload is a key inducer of neuroinflammation and molecular docking predicted a high binding potential between BAA and JAK2, we focused on the classical JAK2/STAT3 inflammatory pathway. The results showed that treatment HT-22 cells with 20 mM Glu for 24 h significantly increased the phosphorylation levels of JAK2 (Tyr1007/1008) and STAT3 (Tyr705), with fold changes of 1.3-fold ($p = 0.0007$ vs Control group) and 1.2-fold ($p = 0.0329$ vs Control group), compared to the Control group. In contrast, BAA treatment significantly suppressed the phosphorylation of both JAK2 and STAT3 (p-JAK2: $p = 0.0350$ (2.5 μM BAA); $p = 0.0243$ (10 μM BAA); p-STAT: $p = 0.049$ (2.5 μM BAA); $p = 0.0012$ (10 μM BAA) vs Glu group). No significant differences were observed in total JAK2 or total STAT3 protein levels among the groups (Figure 7A and B).

qPCR analysis revealed that after 24 h of Glu treatment, the mRNA expression of the inflammatory factors *Tnf-α, Il-6*, and *Il-1β* was significantly upregulated, reaching 5.3-, 3.8-, and 5.1-fold, compared with the Control group (*Tnf-α:* $p = 0.0018$; *Il-6:* $p = 0.0003$; *Il-1β:* $p < 0.0001$ vs Control group). Pretreatment with 10 μM BAA significantly inhibited the expression of these factors, reducing their levels to 1.5 ± 0.5, 1.2 ± 0.2, and 1.3 ± 0.3, respectively, which were not significantly different from the Control group (*Tnf-α:* $p = 0.008$; *Il-6:* $p = 0.0004$; *Il-1β:* $p < 0.0001$ vs Glu group)(Figure 7C). In summary, BAA

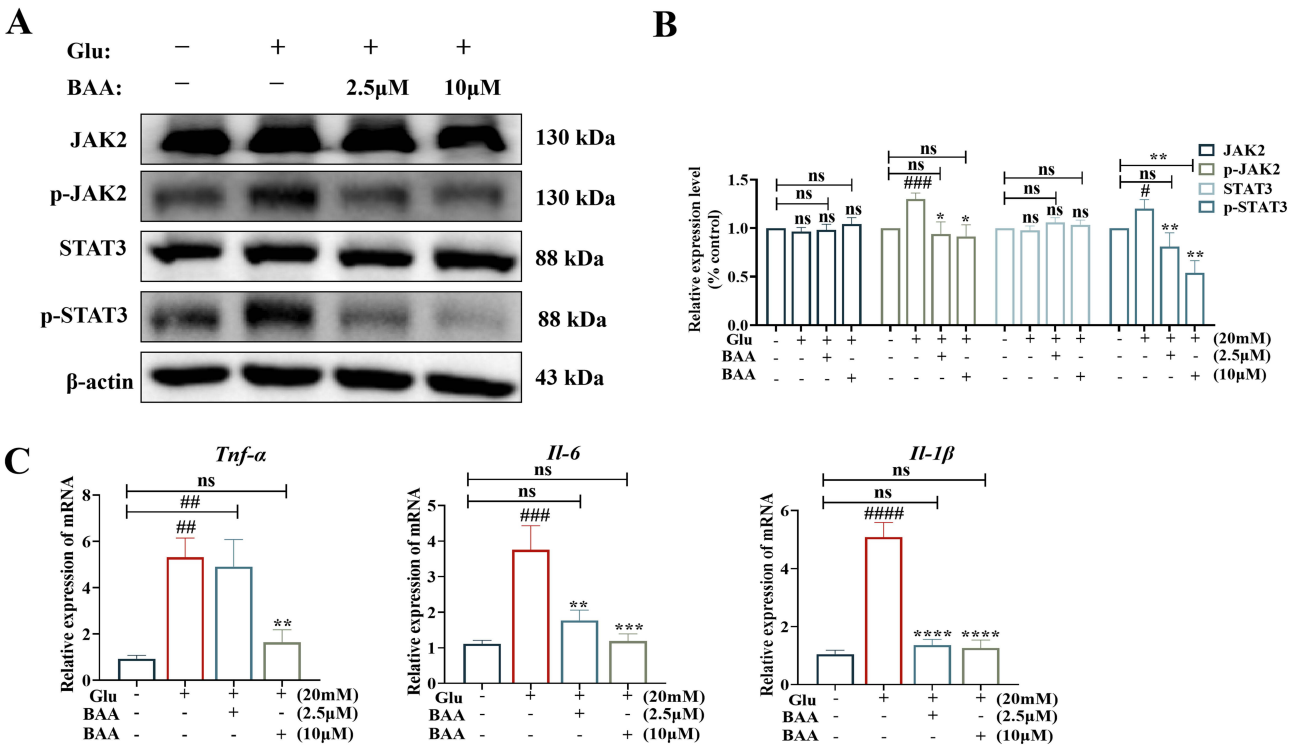

Figure 7 BAA inhibits the JAK2/STAT3 signaling pathway and the gene expression of related inflammatory factors. HT-22 cells were treated with 20 mM Glu alone or in combination with 2.5 μM or 10 μM BAA for 24 h. (**A**) Western blot bands of JAK2, p-JAK2, STAT3, and p-STAT3 proteins; (**B**) Quantification of JAK2, p-JAK2, STAT3, and p-STAT3 protein expression levels. n = 5 independent biological replicates. β-actin was used as the loading control. (**C**) mRNA expression levels of *Tnf-α, Il-6*, and *Il-1β*. n = 6 independent biological replicates. *β-actin* was used as the internal reference. Data are presented as mean ± SEM. Statistical analysis: One-way ANOVA followed by Tukey's post hoc test after establishment of normality (Shapiro–Wilk test) and homogeneity of variance (Levene's test). $^{\#}p < 0.05$, $^{\#\#}p < 0.01$, $^{\#\#\#}p < 0.001$, $^{\#\#\#\#}p < 0.0001$ vs Control group; $^{*}p < 0.05$, $^{**}p < 0.01$, $^{***}p < 0.001$, $^{****}p < 0.0001$ vs Glu group.
Abbreviation: ns, no significant difference.

https://doi.org/10.2147/DDDT.S566649

significantly downregulates the expression of the inflammatory cytokines *Tnf-α, Il-6*, and *Il-1β* by inhibiting the phosphorylation of the JAK2/STAT3 signaling pathway, thereby alleviating neuroinflammatory responses.

Validation of the Ability of BAA to Inhibit Oxidative Stress by Regulating Calcium Homeostasis Using BAPTA-AM

To verify whether the antioxidant effects of BAA depend on calcium homeostasis, a parallel comparison was conducted using the calcium chelator BAPTA-AM. Based on the relevant literature and the CCK-8 assay, the concentration of BAPTA-AM in HT-22 cells was selected as 0.25 μM (Figure 8A).[32] Glu treatment (20 mM, 24 h) significantly induced neuronal damage: Fluo-4 fluorescence intensity rising from 6.80 ± 0.68 to 16.43 ± 0.35 ($p < 0.0001$ vs Control group), ROS fluorescence intensity increased from 4.53 ± 0.38 to 9.73 ± 0.50 ($p < 0.0001$ vs Control group), MDA levels rose from 115.0 ± 1.06 to 150.3 ± 4.83 ($p = 0.0004$ vs Control group), and SOD activity decreased from 21.49 ± 1.78 to 15.15 ± 2.24 ($p = 0.0255$ vs Control group)(Figure 8B–G).

Treatment with 10 μM BAA significantly reversed these effects: Fluo-4 fluorescence intensity decreased to 9.20 ± 0.43 ($p < 0.0001$ vs Glu group), ROS levels decreased to 2.99 ± 0.58 ($p < 0.0001$ vs Glu group), MDA content decreased to 119.6 ± 4.79 ($p = 0.0017$ vs Glu group), and SOD activity increased to 21.07 ± 2.38 ($p = 0.0499$ vs Glu group). Treatment with 0.25 μM BAPTA-AM alone exhibited a protective effect comparable to that of BAA. Fluo-4 fluorescence intensity decreased to 9.68 ±

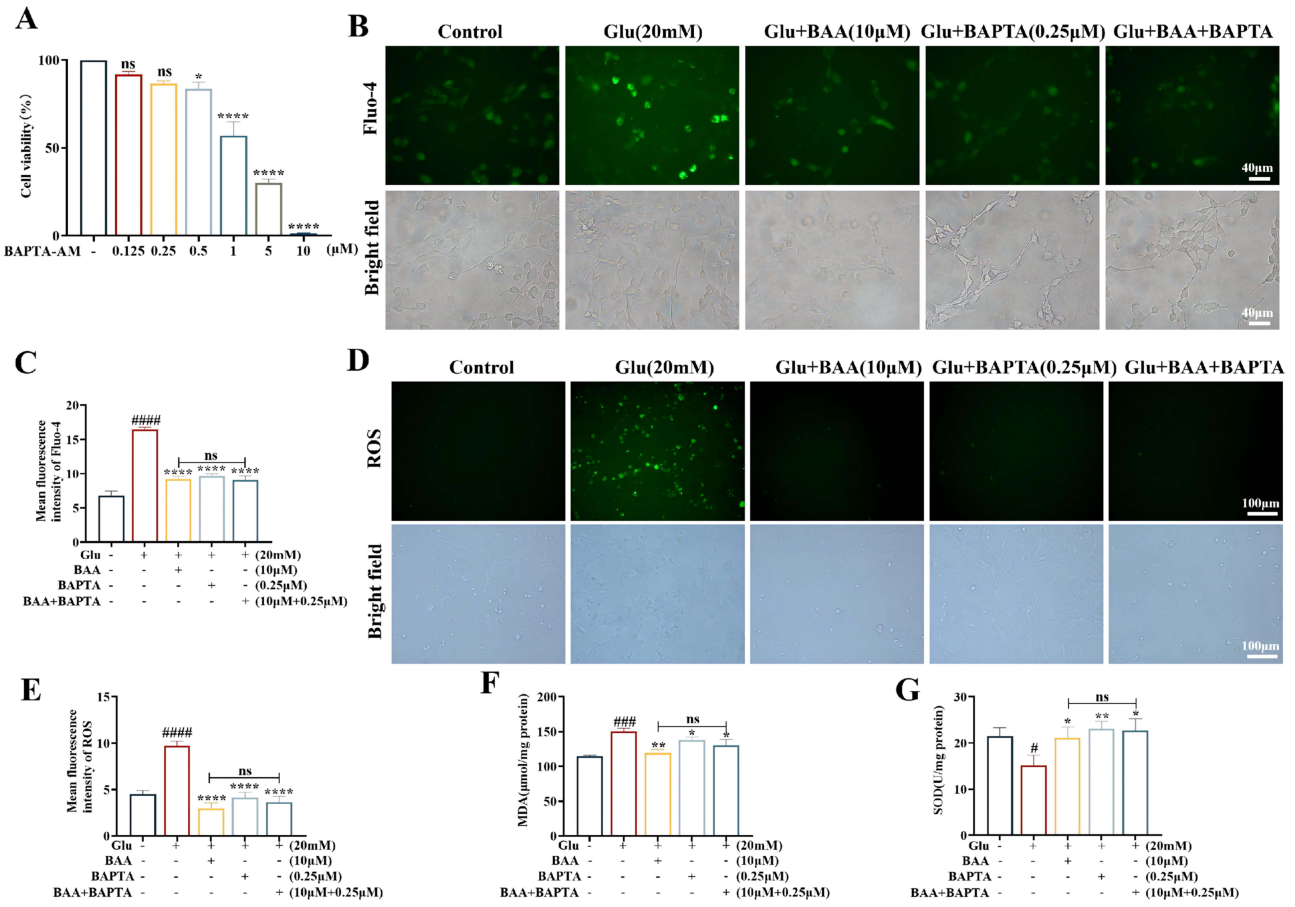

Figure 8 Combining BAA with BAPTA inhibits Glu-induced calcium overload and oxidative stress in HT-22 cells. (**A**)The CCK-8 assay was used to evaluate the effects of different concentrations of BAMPT-AM (0.125, 0.25, 0.5, 1, 5, 10 μM) on the viability of HT-22 cells after 24 h. (**B**) Fluorescence image of Fluo-4 staining (scale bar: 40 μm). Green fluorescence indicates intracellular Ca^{2+} levels. HT-22 cells were exposed to 20 mM Glu for 24 h, treated with 10 μM BAA, 0.25 μM BAPTA-AM, or both. (**C**) Quantitative analysis of Fluo-4 fluorescence intensity; (**D**) Fluorescence image of DCFH-DA staining (scale bar: 100 μm). Green fluorescence indicates ROS levels; (**E**) quantitative analysis of DCFH-DA fluorescence intensity; (**F**) quantitative analysis of MDA content; (**G**) quantitative analysis of SOD activity. Data are presented as mean ± SEM. n = 6 independent biological replicates per group. $^{\#}p < 0.05$, $^{\#\#\#\#}p < 0.001$, $^{\#\#\#\#\#}p < 0.0001$ vs Control group; $^{*}p < 0.05$, $^{**}p < 0.01$, $^{****}p < 0.0001$ vs Glu group. **Abbreviation**: ns, no significant difference.

https://doi.org/10.2147/DDDT.S566649

0.30 ($p < 0.0001$ vs Glu group), ROS levels decreased to 4.14 ± 0.59 ($p < 0.0001$ vs Glu group), MDA content decreased to 138.0 ± 4.40 ($p = 0.0448$ vs Glu group) and SOD activity increased to 23.08 ± 1.62 ($p = 0.0083$ vs Glu group). No significant differences were observed between the BAA and BAA+BAPTA-AM for any of the parameters. These results suggest that BAA and the calcium chelator BAPTA-AM are equally effective in inhibiting calcium overload and oxidative stress, and that their combined use does not produce an additive effect. BAA may exert its antioxidant effects by regulating intracellular calcium homeostasis.

Validation of BAA's Improvement of Mitochondrial Function via Regulation of Calcium Homeostasis Using BAPTA-AM

We investigated whether BAA's protective effect on mitochondrial function depends on the regulation of calcium homeostasis. CCCP (10 μM) was used as a positive control to induce mitochondrial membrane potential depolarization. Compared with the Control group, 20 mM Glu treatment for 24 h significantly reduced mitochondrial membrane potential (MMP), as indicated by a decrease in the JC-1 red/green fluorescence ratio from 42.79 ± 9.52 to 0.25 ± 0.023 ($p < 0.0001$ vs Control group), and depleted ATP levels from 71.74 ± 2.62 to 47.88 ± 0.68 ($p < 0.0001$ vs Control group) (Figure 9A–C). Treatment with 10 μM

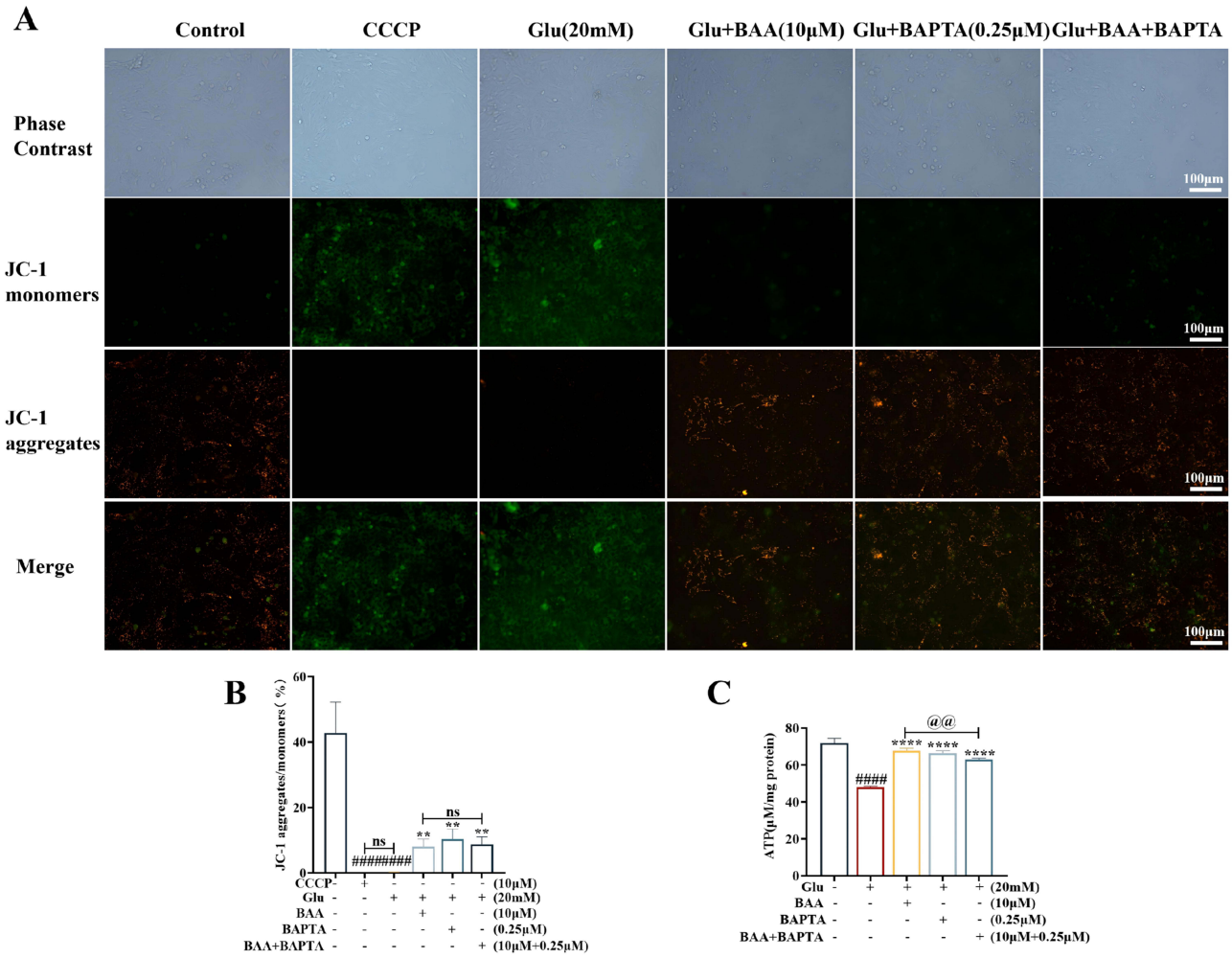

Figure 9 BAA in combination with BAPTA-AM improves glutamate-induced mitochondrial dysfunction by regulating calcium homeostasis. HT-22 cells were treated with 20 mM Glu for 24 h, with concurrent administration of 10 μM BAA and/or 0.25 μM BAPTA-AM. (**A**) Fluorescence image of JC-1 staining (scale bar: 100 μm); red fluorescence indicates JC-1 aggregates (high membrane potential), and green fluorescence indicates JC-1 monomers (low membrane potential); CCCP (10 μM) was used as a positive control to validate the JC-1 staining assay; (**B**) Quantitative analysis of the JC-1 aggregates/monomers fluorescence ratio; (**C**) Quantitative analysis of intracellular ATP levels. Data are presented as mean ± SEM. n = 6 independent biological replicates per group. $^{\#\#\#\#}p < 0.0001$ vs Control group; $^{**}p < 0.01$, $^{****}p < 0.0001$ vs Glu group; $^{@@}p < 0.01$ vs BAA + BAPTA-AM group.

Abbreviation: ns, no significant difference.

BAA significantly reversed these effects, restoring the JC-1 ratio to 8.06 ± 2.30 ($p = 0.0034$ vs Glu group) and ATP levels to 67.69 ± 1.36 ($p < 0.0001$ vs Glu group). Treatment with 0.25 μM BAPTA-AM alone exhibited comparable protective effects, restoring the JC-1 ratio to 10.37 ± 3.07 ($p = 0.004$ vs Glu group) and ATP levels to 66.17 ± 1.48 ($p < 0.0001$ vs Glu group). No significant difference was observed in the JC-1 ratio between BAA and BAA + BAPTA-AM groups. In contrast, ATP levels were significantly lower in BAA + BAPTA-AM group compared to BAA group ($p = 0.0054$ vs BAA group). Collectively, these results support that BAA improves mitochondrial function largely through regulation of calcium homeostasis, with potential involvement of additional calcium-independent pathways in ATP synthesis.

Validation of BAA's Inhibition of Cell Apoptosis and the JAK2/STAT3 Pathway via Regulation of Calcium Homeostasis Using BAPTA-AM

We investigated whether BAA's inhibition of downstream apoptosis and JAK2/STAT3 singling pathways depends on calcium homeostasis regulation using BAPTA-AM. Flow cytometry results showed that Glu treatment significantly increased the apoptosis rate by 8.1-fold (24.34 ± 1.05%) compared with the Control group (2.99 ± 0.21%)($p < 0.0001$ vs Control group). Pretreatment with 10 μM BAA, 0.25 μM BAPTA, or both reduced the apoptosis rate to 2.8-, 2.6-, and 3.0-fold that of the control group (all, $p < 0.0001$ vs Glu group)(Figure 10A and B).

Western blot analysis revealed that Glu treatment significantly increased p-JAK2 and p-STAT3 levels ($p = 0.0034$ and $p < 0.0001$, respectively, vs Glu group). Pretreatment with 10 μM BAA significantly inhibited Glu-induced p-JAK2 and

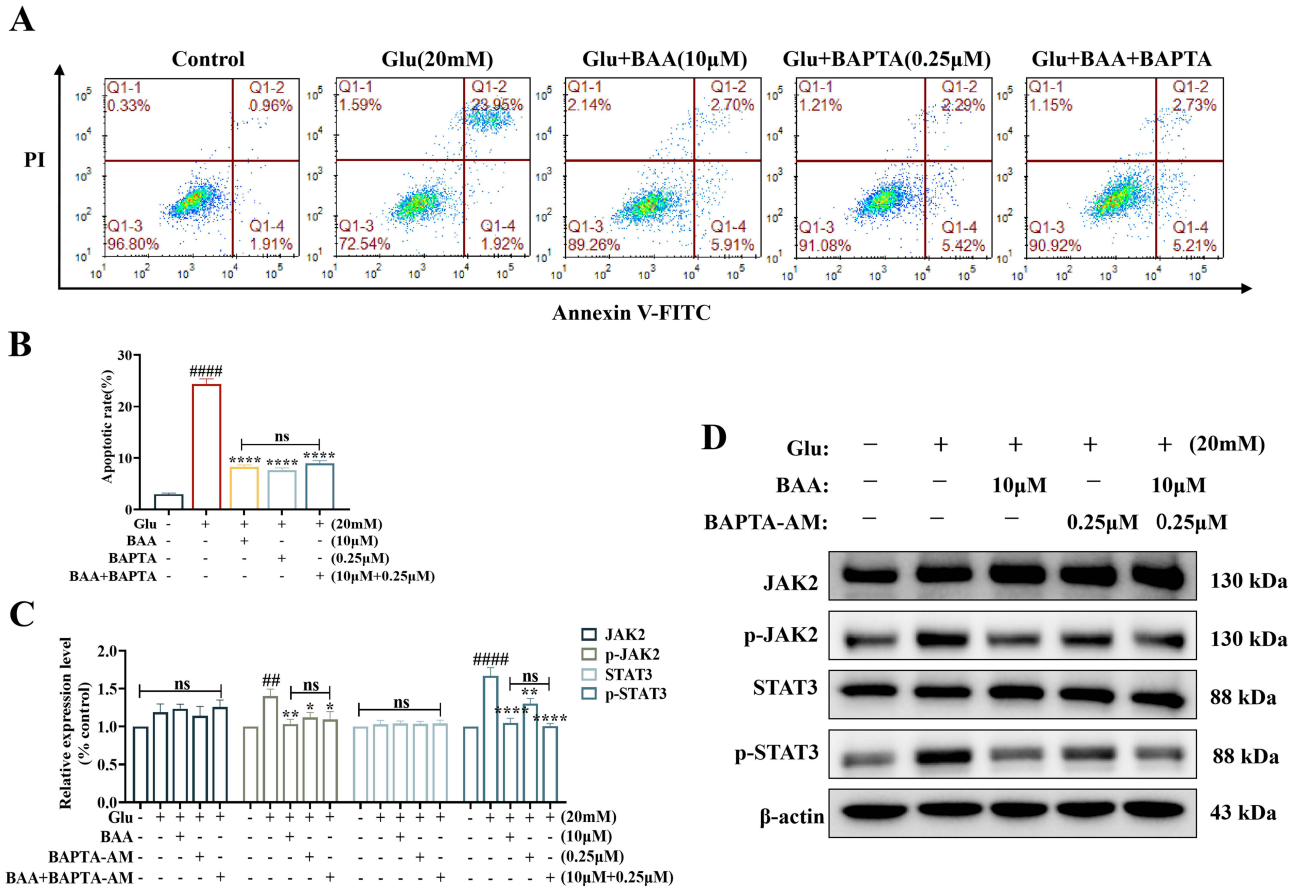

Figure 10 Regulation of glutamate-induced apoptosis and the JAK2/STAT3 signaling pathway by BAA in combination with BAPTA-AM. HT-22 cells were treated with 20 mM Glu for 24 h, with concurrent administration of 10 μM BAA and/or 0.25 μM BAPTA-AM. (**A**) Flow cytometry dot plot of Annexin V-FITC/PI double staining. Quadrant definitions: Q1: Necrotic cells (Annexin V^-/PI^+); Q2: Late apoptotic cells (Annexin V^+/PI^+); Q3: Viable cells (Annexin V^-/PI^-); Q4: Early apoptotic cells (Annexin V^+/PI^-); (**B**) Quantitative analysis of total apoptosis rate (Q2+Q4). n = 6 independent biological replicates. (**C**) Quantitative of JAK2, p-JAK2, STAT3, and p-STAT3 protein expression; (**D**) Western blot analysis for JAK2, p-JAK2, STAT3, and p-STAT3 proteins, with β-actin as the internal control. n = 5 independent biological replicates. Data are presented as mean ± SEM. $^{\#\#}p < 0.01$; $^{\#\#\#\#}p < 0.0001$ vs Control group; $^{*}p < 0.05$; $^{**}p < 0.01$, $^{****}p < 0.0001$ vs Glu group.

Abbreviation: ns, no significant difference.

https://doi.org/10.2147/DDDT.S566649

p-STAT3 levels ($p = 0.0071$ and $p < 0.0001$, respectively, vs Glu group). Similarly, 0.25 μM BAPTA-AM alone also suppressed JAK2/STAT3 activation (p-JAK2: $p = 0.0448$; p-STAT3: $p = 0.0027$, vs Glu group). Notably, combined treatment with BAA and BAPTA-AM did not produce an additive inhibitory effect. No significant differences were observed in total JAK2 or STAT3 protein levels among groups (Figure 10C and D). These findings further suggest that BAA inhibits apoptosis and JAK2/STAT3 signaling by regulating calcium homeostasis.

Discussion

The essence of epileptic seizures lies in the abnormal, synchronous excessive discharge of neurons in the brain. Pathological hyperexcitability can lead not only to acute behavioral and cognitive impairments but also to long-term neurodegeneration, reduced quality of life, and an increased risk of injury and sudden unexpected death in epilepsy.[33] BAA is an acetylated derivative of β-amyrin, a natural pentacyclic triterpenoid. Studies have shown that β-amyrin exerts antiepileptic effects through mechanisms such as reducing oxidative stress and inflammation.[6,34] Compared with the parent compound, acetylation significantly reduces the polarity of BAA while enhancing its lipophilicity.[9] Structurally similar pentacyclic triterpenoids (eg, ursolic acid) have been reported to exhibit markedly improved bioavailability following acetylation.[35] Based on these observations, we hypothesize that BAA may possess the ability to penetrate the BBB, providing a theoretical rationale for its efficacy in antiepileptic models. In this study, we systematically evaluated the antiepileptic effects of BAA and its underlying neuroprotective mechanisms. Using a PTZ-induced zebrafish epilepsy model and a Glu-induced HT-22 neuronal injury model, we suggest that BAA exerts multi-target antiepileptic effects by inhibiting neuronal calcium overload, alleviating oxidative stress, mitochondrial dysfunction, neuroinflammation, and apoptosis. These findings provide experimental support for the development of BAA as a promising antiepileptic candidate.

Zebrafish, characterized by rapid reproduction and a high degree of genetic homology with humans, have become a widely used model organism in epilepsy research. They are suitable for high-throughput drug screening, behavioral analysis, electroencephalography (EEG) recording, and in vivo imaging, and can model various types of genetic and acquired epilepsy.[36] In the zebrafish model, PTZ induces seizures by antagonizing GABA_A receptors associated with chloride channels, triggering a series of concentration-dependent behavioral changes that ultimately manifest as clonic-like convulsions.[37] In our research, PTZ exposure significantly increased total swimming distance, average speed, and tonic-clonic seizure frequency in zebrafish larvae, whereas pretreatment with BAA significantly reduced all these parameters. Notably, BAA was more effective than the positive control VPA in suppressing swimming speed.

In PTZ-induced epilepsy models and clinical patients, Glu concentrations in the brain are significantly elevated, making it one of the key factors contributing to neuronal damage.[38] Excessive Glu release not only mediates excito-toxicity but also triggers neuroinflammation. As a core excitatory neurotransmitter, Glu excessively activates NMDA receptors on the postsynaptic membrane, causing massive Ca^{2+} influx and leading to intracellular "calcium overload." Calcium overload subsequently triggers a series of deleterious events: disruption of mitochondrial function, activation of calcium-dependent enzymes (such as nitric oxide synthase and phospholipases), a sharp increase in ROS production, and severe oxidative stress. ROS further attack phospholipids in the cell membrane to produce lipid peroxides (such as MDA) and, through hydroxyl radicals, oxidize nuclear and mitochondrial DNA, activating the PARP pathway and causing energy depletion. Furthermore, ROS can upregulate the expression of the pro-apoptotic protein Bax, induce the opening of the mitochondrial porin, trigger the release of cytochrome C, and activate the caspase cascade, ultimately leading to apoptosis.[27,39,40] Notably, calcium overload and ROS bursts are also key factors in activating pro-inflammatory pathways such as NF-κB, which can further exacerbate neuroinflammatory responses.

To further investigate the antiepileptic potential of BAA, we examined changes in ROS levels, apoptosis, and inflammatory factors in zebrafish. Studies have demonstrated that PTZ induces ROS accumulation, increased apoptosis, and the upregulation of inflammatory factors (such as TNF-α, IL-6, IL-1β and COX-2) in zebrafish.[41–43] COX-2 is a key driver of the post-seizure neuroinflammatory response. It is rapidly induced in hippocampal and cortical neurons within hours of a seizure, and catalyses the conversion of arachidonic acid into prostaglandin H_2 (PGH_2). Cell-specific synthases then convert PGH_2 into prostaglandins, including PGE_2, PGD_2, and $PGF_2\alpha$. These prostaglandins activate corresponding G protein-coupled receptors, thereby mediating neuroinflammation, disruption of the BBB, and neuronal damage.[44]

However, research findings on the use of selective COX-2 inhibitors (such as celecoxib and rofecoxib) in epilepsy models have been inconsistent. Some studies have indicated neuroprotective effects,[45,46] while others have not observed clear benefits, and some have even demonstrated pro-convulsant effects.[47] Unlike direct COX-2 targeting, BAA acts on calcium homeostasis further upstream, potentially avoiding the cardiovascular risks associated with direct COX-2 inhibition.[48] In addition, classical antioxidants (such as N-acetylcysteine, NAC) primarily scavenge ROS directly by replenishing glutathione and have demonstrated protective effects in epilepsy models.[49] However, the action of NAC is primarily confined to downstream stages of oxidative stress, and its regulation of calcium overload and subsequent inflammatory pathways is relatively indirect.[50] In contrast, while the antiepileptic neuroprotective effects of BAA overlap phenotypically with those of classic anti-inflammatory or antioxidant drugs, its mechanism of action emphasises the regulation of calcium homeostasis and the multilevel blockade of the "calcium-oxidative stress-inflammation" cascade. BAA may be suitable for subtypes of refractory epilepsy driven by calcium homeostasis imbalance, providing a theoretical basis for its development as a novel multi-target candidate compound.

Our research further revealed that BAA significantly inhibits calcium overload induced by Glu in HT-22 cells. The effect of BAA is comparable to that of the calcium chelator BAPTA-AM, and no additional effect was observed when the two were combined. This suggests that the protective effect of BAA primarily depends on its regulation of intracellular calcium homeostasis. Notably, in excitotoxicity models, intracellular calcium overload in neurons does not solely depend on the activation of voltage-gated calcium channels or NMDA receptors. Growing evidence indicates that store-operated calcium entry (SOCE) is a critical component of this process. SOCE is triggered by calcium depletion in the endoplasmic reticulum and senses changes in calcium concentration via Stromal Interaction Molecule (STIM) proteins (eg. STIM1). These proteins then activate Orai channels on the plasma membrane, mediating sustained calcium influx.[51–53] In epilepsy models, abnormal SOCE activation has been shown to enhance neuronal excitability, promote synchronised discharges and exacerbate epileptic susceptibility.[53,54] In HT-22 cells in particular, where functional NMDA receptors are absent, Glu-induced calcium overload primarily relies on oxidative stress-induced endoplasmic reticulum calcium depletion and subsequent SOCE activation.[51,52] Therefore, we hypothesise that BAA may suppress pathological calcium influx by interfering with the STIM/Orai-mediated SOCE pathway. Our future studies should employ techniques such as gene knockdown (eg, siRNA targeting STIM1/Orai1) or specific SOCE inhibitors to clarify BAA's regulatory role in the SOCE pathway and its molecular targets.

The "ROS–Ca^{2+}" positive feedback loop is not only a core mechanism regulating neuronal redox status and calcium homeostasis, but has also been suggested as a key upstream event directly activating the JAK2/STAT3 signaling pathway.[55] Unlike the classical cytokine-mediated activation pathway (eg, IL-6 binding to extracellular domains of membrane receptors and inducing JAK dimerization), this mode of activation exhibits distinct non-cytokine-dependent characteristics. JAK2 belongs to the non-receptor tyrosine kinase family, and the JAK-STAT signaling pathway is involved in epileptogenesis and progression through multiple processes, including modulation of neuronal excitability, synaptic plasticity, glial cell activation, and neuroinflammatory responses.[56,57] Activated JAK2/STAT3 signaling promotes the expression of downstream inflammatory factors. These highly expressed inflammatory factors, in turn, bind to their receptors and further activate JAK2 and STAT3, promoting their phosphorylation and sustaining inflammatory amplification.[58] Kong et al found that activation of the JAK2/STAT3 pathway significantly exacerbates neuroinflammation[59] In addition, downstream signals regulated by JAK2/STAT3 include apoptosis-related targets such as Caspase-3 and Bax/Bcl-2 family proteins, thereby aggravating neuronal apoptosis. Hu et al reported that inhibition of the JAK2/STAT3 pathway alleviates epilepsy-induced brain injury[60] Hong et al, demonstrated that the JAK1/2 inhibitor AZD1480 suppresses inflammatory gene expression in microglia and macrophages by inhibiting JAK2/STAT3 signaling[61] Notably, clinically used JAK inhibitors (such as tofacitinib) not only suppress seizures but also improve cognitive function, showing potential as adjunctive therapy for epilepsy.[62] Combined with molecular docking results indicating high binding affinity between BAA and JAK2, we hypothesize that BAA may act as a novel JAK2/STAT3 pathway inhibitor, exerting multi-target anti-neuroinflammatory and anti-apoptotic effects in epilepsy through intervention in this signaling axis.

Although this study has yielded some findings, certain limitations remain. While BAA exhibits high lipophilicity, its poor water solubility poses challenges for formulation development and systemic administration. Nanoparticle formulations hold promise for enhancing their bioavailability and enabling targeted delivery to the central nervous system, such

as liposomes and nanoemulsions. The ability of BAA to cross the BBB requires experimental validation using models such as the parallel artificial membrane permeability assay for the BBB (PAMPA-BBB), Madin-Darby canine kidney cells (MDCK-MDR1) transfected with human multidrug resistance protein 1 (MDR1), or distribution in zebrafish brain tissue. Molecular docking results need to be validated using direct binding assay techniques such as surface plasmon resonance (SPR) or microcalorimetry (MST). Current conclusions are primarily based on zebrafish and HT-22 cell models. Future studies should further validate their translational potential in primary neurons and mammalian epilepsy models, such as PTZ-induced epileptic mice and the pilocarpine-induced temporal lobe epilepsy model. The possibility that BAA may exert nonspecific central nervous system depressant or immunomodulatory effects has not yet been ruled out. Further studies using behavioral and molecular assays are needed to clarify its target specificity. In addition, the potential for BAA to act synergistically with or serve as an adjunct to standard antiepileptic drugs (AEDs) remains to be explored. The specific mechanisms of interaction between BAA and calcium-regulatory proteins (such as STIM/Orai channels) require further investigation using gene knockout and electrophysiological techniques.

Conclusion

Our research is the first to reveal the antiepileptic effects of BAA and its multi-target neuroprotective mechanisms. In a PTZ-induced zebrafish epilepsy model, BAA significantly suppressed epileptic-like behavior and alleviated oxidative stress, apoptosis, and neuroinflammatory responses. Network pharmacology and molecular docking predicted calcium signaling pathways, as well as JAK2 and Bcl-2, as potential targets of action. In vitro experiments further suggested that BAA alleviates Glu-induced calcium overload in HT-22 cells, downregulates the Bax/Bcl-2 ratio, and inhibits the excessive activation of the JAK2/STAT3 signaling pathway, thereby reducing neuronal apoptosis and inflammatory responses. Co-treatment with BAPTA-AM further validated that the protective effect of BAA depends on the regulation of intracellular calcium homeostasis. In summary, BAA exerts its antiepileptic effects by inhibiting neuronal calcium overload, regulating the JAK2/STAT3 signaling pathway, and blocking the cascade of neuroinflammation and apoptosis. However, the current conclusions are primarily based on phenotypic observations and network pharmacology inferences, and the mechanism of action requires further experimental validation. Future studies should verify its universality across various epilepsy models and employ molecular biology and gene editing technologies to elucidate its specific targets and regulatory mechanisms.

Data Sharing Statement

The data used to support the findings of this study are available from the corresponding authors upon request.

Author Contributions

All authors made a significant contribution to the work reported, whether that is in the conception, study design, execution, acquisition of data, analysis and interpretation, or in all these areas; took part in drafting, revising or critically reviewing the article; gave final approval of the version to be published; have agreed on the journal to which the article has been submitted; and agree to be accountable for all aspects of the work.

Funding

We acknowledge the funding provided by National Natural Sciences Foundation of China (No.82074016, No.81603296); Program of Jiangsu Administration of Traditional Chinese Medicine (No.2020ZX18, No.ZD202527); Science and Technology Plan of Changzhou (No. CM20223006, No. CJ20252044, No.CJ20229010); Scientific Research Fund Project of Jiangsu Geriatrics Society (No. JGS2025ZD007); Changzhou "Longcheng Qiangyi" Project - Traditional Chinese Medicine Talent Cultivation Program: Zhang Bing Qihuang Scholar Studio (Changcai She[2024] No.55); Postgraduate Research & Practice Innovation Program of Jiangsu Province (SJCX24_0917).

Disclosure

The author(s) report no conflicts of interest in this work.

References

1. Li C, Wang X, Deng M, et al. Antiepileptic drug combinations for epilepsy: mechanisms, clinical strategies, and future prospects. *Int J Mol Sci*. 2025;26(9). doi:10.3390/ijms26094035
2. Scheffer IE, Berkovic S, Capovilla G, et al. ILAE classification of the epilepsies: position paper of the ILAE commission for classification and terminology. *Epilepsia*. 2017;58(4):512–521. doi:10.1111/epi.13709
3. Ratnaike T, Elkhateeb N, Lochm C, et al. Evidence for sodium valproate toxicity in mitochondrial diseases: a systematic analysis. *BMJ Neurol Open*. 2024;6(1):e000650. doi:10.1136/bmjno-2024-000650
4. Wu J, Cao M, Peng Y, et al. Research progress on the treatment of epilepsy with traditional Chinese medicine. *Phytomedicine*. 2023;120:155022. doi:10.1016/j.phymed.2023.155022
5. Okoye NN, Ajaghaku DL, Okeke HN, et al. β-amyrin and α-amyrin acetate isolated from the stem bark of Alstonia boonei display profound anti-inflammatory activity. *Pharm Biol*. 2014;52(11):1478–1486. doi:10.3109/13880209.2014.898078
6. Aragão GF, Carneiro LM, Rota-Junior AP, et al. Alterations in brain amino acid metabolism and inhibitory effects on PKC are possibly correlated with anticonvulsant effects of the isomeric mixture of α- and β-amyrin from Protium heptaphyllum. *Pharm Biol*. 2015;53(3):407–413. doi:10.3109/13880209.2014.923001
7. Henneh I, Biney R, Acheampong S, et al. Anti-epileptogenic activity of ziziphus abyssinica root bark extract and its isolated bioactive compound, β-amyrin. *IBRO Neurosci Rep*. 2023;15:S578. doi:10.1016/j.ibneur.2023.08.1145
8. Angsusing J, Singh S, Samee W, et al. Anti-inflammatory activities of yataprasen thai traditional formulary and its active compounds, β-amyrin and stigmasterol, in RAW264.7 and THP-1 Cells. *Pharmaceuticals*. 2024;17(8):1018. doi:10.3390/ph17081018
9. Lipinski CA, Lombardo F, Dominy BW, et al. Experimental and computational approaches to estimate solubility and permeability in drug discovery and development settings. *Adv Drug Deliv Rev*. 2001;46(1–3):3–26. doi:10.1016/s0169-409x(00)00129-0
10. Choi-Sledeski Y, Wermuth C. Chapter 28 - designing prodrugs and bioprecursors. In: Wermuth CG, Aldous D, Raboisson P, editors. *The Practice of Medicinal Chemistry*. 4th ed. San Diego: Academic Press; 2015:657–696.
11. Sumadewi K, Harkitasari S, Tjandra D. Biomolecular mechanisms of epileptic seizures and epilepsy: a review. *Acta Epileptol*. 2023;5(1):28. doi:10.1186/s42494-023-00137-0
12. Staley K. Molecular mechanisms of epilepsy. *Nat Neurosci*. 2015;18(3):367–372. doi:10.1038/nn.3947
13. Olsen R. $GABA_A$ receptor: positive and negative allosteric modulators. *Neuropharmacology*. 2018;136:10–22. doi:10.1016/j.neuropharm.2018.01.036
14. Chen TS, Huang TH, Lai MC, et al. The role of glutamate receptors in epilepsy. *Biomedicines*. 2023;11(3):783. doi:10.3390/biomedicines11030783
15. Parsons ALM, Bucknor EMV, Castroflorio E, et al. The interconnected mechanisms of oxidative stress and neuroinflammation in epilepsy. *Antioxidants*. 2022;11(1):157. doi:10.3390/antiox11010157
16. Simon AR, Vikis HG, Stewart S, et al. Regulation of STAT3 by direct binding to the Rac1 GTPase. *Science*. 2000;290(5489):144–147. doi:10.1126/science.290.5489.144
17. Liu D, Lin J, Su J, et al. Glutamine deficiency promotes PCV2 infection through induction of autophagy via activation of ROS-mediated JAK2/STAT3 signaling pathway. *J Agric Food Chem*. 2018;66(44):11757–11766. doi:10.1021/acs.jafc.8b04704
18. Jia F, Liu Y, Dou X, et al. Liensinine inhibits osteosarcoma growth by ROS-Mediated suppression of the JAK2/STAT3 signaling pathway. *Oxid Med Cell Longev*. 2022;2022:8245614. doi:10.1155/2022/8245614
19. D'Amora M, Galgani A, Marchese M, et al. Zebrafish as an innovative tool for epilepsy modeling: state of the art and potential future directions. *Int J Mol Sci*. 2023;24(9):7702. doi:10.3390/ijms24097702
20. Okanari K, Teranishi H, Umeda R, et al. Behavioral and neurotransmitter changes on antiepileptic drugs treatment in the zebrafish pentylenetetrazol-induced seizure model. *Behav Brain Res*. 2024;464:114920. doi:10.1016/j.bbr.2024.114920
21. Fontana BD, Blanco L, Uchoa AE, et al. Development and applications of a machine learning model for an in-depth analysis of pentylenetetrazol-induced seizure-like behaviors in adult zebrafish. *Neuroscience*. 2025;568:377–387. doi:10.1016/j.neuroscience.2025.01.048
22. Afrikanova T, Serruys AS, Buenafe OE, et al. Validation of the zebrafish pentylenetetrazol seizure model: locomotor versus electrographic responses to antiepileptic drugs. *PLoS One*. 2013;8(1):e54166. doi:10.1371/journal.pone.0054166
23. Fleming A, Diekmann H, Goldsmith P. Functional characterisation of the maturation of the blood-brain barrier in larval zebrafish. *PLoS One*. 2013;8(10):e77548. doi:10.1371/journal.pone.0077548
24. Shaw PAG, Panda SK, Stanca A, et al. Optimization of a locomotion-based zebrafish seizure model. *J Neurosci Methods*. 2022;375:109594. doi:10.1016/j.jneumeth.2022.109594
25. Shin JN, Lee KB, Butterworth W, et al. Zebrafish EEG predicts the efficacy of antiepileptic drugs. *Front Pharmacol*. 2022;13:1055424. doi:10.3389/fphar.2022.1055424
26. Liu Y, Shen T, Li Q, et al. Various gases for the treatment of neuropathic pain: mechanisms, current status, and future perspectives. *Med Gas Res*. 2025;15(4):488–495. doi:10.4103/mgr.MEDGASRES-D-24-00161
27. Yang N, Guan QW, Chen FH, et al. Antioxidants targeting mitochondrial oxidative stress: promising neuroprotectants for epilepsy. *Oxid Med Cell Longev*. 2020;2020:6687185. doi:10.1155/2020/6687185
28. Méndez-Armenta M, Nava-Ruíz C, Juárez-Rebollar D, et al. Oxidative stress associated with neuronal apoptosis in experimental models of epilepsy. *Oxid Med Cell Longev*. 2014;2014:293689. doi:10.1155/2014/293689
29. Kiessling M, Gass P. Immediate early gene expression in experimental epilepsy. *Brain Pathol*. 1993;3(4):381–393. doi:10.1111/j.1750-3639.1993.tb00766.x
30. Magalhães SA, Foresti ML, Barros VN, et al. Marmosets have a greater diversity of c-Fos response after hyperstimulation in distinct cortical regions as compared to rats. *J Comp Neurol*. 2021;529(7):1628–1641. doi:10.1002/cne.25044
31. Cao C, Mu J, Hu G, et al. A correlation between inflammatory factors and epileptic seizures: a meta-analysis. *Actas Esp Psiquiatr*. 2025;53(4):902–913. doi:10.62641/aep.v53i4.1790
32. Lee DG, Park J, Lee HS, et al. Iron overload-induced calcium signals modulate mitochondrial fragmentation in HT-22 hippocampal neuron cells. *Toxicology*. 2016;365:17–24. doi:10.1016/j.tox.2016.07.022
33. Hashmi SA, Gundlapalli R, Zawar I. Mortality in older adults with epilepsy: an understudied entity. *Epilepsia Open*. 2025;10(1):15–30. doi:10.1002/epi4.13098

34. Nogueira AO, Oliveira YIS, Adjafre BL, et al. Pharmacological effects of the isomeric mixture of alpha and beta amyrin from Protium heptaphyllum: a literature review. *Fundam Clin Pharmacol*. 2019;33(1):4–12. doi:10.1111/fcp.12402
35. AlQathama A, Shao L, Bader A, et al. Differential anti-proliferative and anti-migratory activities of ursolic acid, 3-o-acetylursolic acid and their combination treatments with quercetin on melanoma cells. *Biomolecules*. 2020;10(6):894. doi:10.3390/biom10060894
36. Gawel K, Langlois M, Martins T, et al. Seizing the moment: zebrafish epilepsy models. *Neurosci Biobehav Rev*. 2020;116:1–20. doi:10.1016/j.neubiorev.2020.06.010
37. Baraban SC, Taylor MR, Castro PA, et al. Pentylenetetrazole induced changes in zebrafish behavior, neural activity and c-fos expression. *Neuroscience*. 2005;131(3):759–768. doi:10.1016/j.neuroscience.2004.11.031
38. Zhao X, Cheng P, Xu R, et al. Insights into the development of pentylenetetrazole-induced epileptic seizures from dynamic metabolomic changes. *Metab Brain Dis*. 2022;37(7):2441–2455. doi:10.1007/s11011-022-01018-0
39. Lewerenz J, Hewett SJ, Huang Y, et al. The cystine/glutamate antiporter system x(c)(-) in health and disease: from molecular mechanisms to novel therapeutic opportunities. *Antioxid Redox Signal*. 2013;18(5):522–555. doi:10.1089/ars.2011.4391
40. Valero T. Mitochondrial biogenesis: pharmacological approaches. *Curr Pharm Des*. 2014;20(35):5507–5509. doi:10.2174/1381612820351409111421 18
41. Manish R, Brindha D, Deenathayalan U. Behavioral rescue: naringenin's neuroprotective effects against PTZ-induced seizures by mitigating oxidative stress and neuroinflammation in zebrafish larvae. *Pharmacol Res Mod Chin Med*. 2024;12:100459. doi:10.1016/j.prmcm.2024.100459
42. Murugan R, Ramya Ranjan Nayak S, Haridevamuthu B, et al. Neuroprotective potential of pyrazole benzenesulfonamide derivative T1 in targeted intervention against PTZ-induced epilepsy-like condition in in vivo zebrafish model. *Int Immunopharmacol*. 2024;131:111859. doi:10.1016/j.intimp.2024.111859
43. Kim SS, Kan H, Hwang KS, et al. Neurochemical effects of 4-(2chloro-4-fluorobenzyl)-3-(2-thienyl)-1,2,4-oxadiazol-5(4H)-one in the pentylenetetrazole (PTZ)-induced epileptic seizure zebrafish model. *Int J Mol Sci*. 2021;22(3):1285. doi:10.3390/ijms22031285
44. Rojas A, Chen D, Ganesh T, et al. The COX-2/prostanoid signaling cascades in seizure disorders. *Expert Opin Ther Targets*. 2019;23(1):1–13. doi:10.1080/14728222.2019.1554056
45. Kunz T, Oliw EH. The selective cyclooxygenase-2 inhibitor rofecoxib reduces kainate-induced cell death in the rat hippocampus. *Eur J Neurosci*. 2001;13(3):569–575. doi:10.1046/j.1460-9568.2001.01420.x
46. Gobbo OL, O'Mara SM. Post-treatment, but not pre-treatment, with the selective cyclooxygenase-2 inhibitor celecoxib markedly enhances functional recovery from kainic acid-induced neurodegeneration. *Neuroscience*. 2004;125(2):317–327. doi:10.1016/j.neuroscience.2004.01.045
47. Taşkıran M, Taşdemir A, Ayyıldız N. Acute effects of aceclofenac, COX-2 inhibitor, on penicillin-induced epileptiform activity. *Brain Res Bull*. 2017;130:42–46. doi:10.1016/j.brainresbull.2016.12.010
48. Arehart E, Stitham J, Asselbergs FW, et al. Acceleration of cardiovascular disease by a dysfunctional prostacyclin receptor mutation: potential implications for cyclooxygenase-2 inhibition. *Circ Res*. 2008;102(8):986–993. doi:10.1161/circresaha.107.165936
49. Chitolina R, Reis CG, Stahlhofer-Buss T, et al. Effects of N-acetylcysteine and acetyl-L-carnitine on acute PTZ-induced seizures in larval and adult zebrafish. *Pharmacol Rep*. 2023;75(6):1544–1555. doi:10.1007/s43440-023-00536-7
50. Deepmala, Slattery J, Kumar N, et al. Clinical trials of N-acetylcysteine in psychiatry and neurology: a systematic review. *Neurosci Biobehav Rev*. 2015;55:294–321. doi:10.1016/j.neubiorev.2015.04.015
51. Li X, Tao AL, Wu N, et al. Calcium-iron crosstalk in epileptogenesis: unraveling mechanisms and therapeutic opportunities. *Neurobiol Dis*. 2025;212:106989. doi:10.1016/j.nbd.2025.106989
52. Courjaret R, Prakriya M, Machaca K. SOCE as a regulator of neuronal activity. *J Physiol*. 2024;602(8):1449–1462. doi:10.1113/jp283826
53. Hori K, Tsujikawa S, Novakovic MM, et al. Regulation of chemoconvulsant-induced seizures by store-operated Orai1 channels. *J Physiol*. 2020;598(23):5391–5409. doi:10.1113/jp280119
54. Steinbeck JA, Henke N, Opatz J, et al. Store-operated calcium entry modulates neuronal network activity in a model of chronic epilepsy. *Exp Neurol*. 2011;232(2):185–194. doi:10.1016/j.expneurol.2011.08.022
55. Duhé RJ. Redox regulation of Janus kinase: the elephant in the room. *JAK-STAT*. 2013;2(4):e26141. doi:10.4161/jkst.26141
56. Sun H, Ma D, Cheng Y, et al. The JAK-STAT signaling pathway in epilepsy. *Curr Neuropharmacol*. 2023;21(10):2049–2069. doi:10.2174/1570159x21666221214170234
57. Sopjani M, Morina R, Uka V, et al. JAK2-mediated intracellular signaling. *Curr Mol Med*. 2021;21(5):417–425. doi:10.2174/1566524020666201015144702
58. Yin Q, Zhao B, Zhu J, et al. JLX001 improves myocardial ischemia-reperfusion injury by activating Jak2-Stat3 pathway. *Life Sci*. 2020;257:118083. doi:10.1016/j.lfs.2020.118083
59. Kong X, Gong Z, Zhang L, et al. JAK2/STAT3 signaling mediates IL-6-inhibited neurogenesis of neural stem cells through DNA demethylation/methylation. *Brain Behav Immun*. 2019;79:159–173. doi:10.1016/j.bbi.2019.01.027
60. Hu QP, Yan HX, Peng F, et al. Genistein protects epilepsy-induced brain injury through regulating the JAK2/STAT3 and Keap1/Nrf2 signaling pathways in the developing rats. *Eur J Pharmacol*. 2021;912:174620. doi:10.1016/j.ejphar.2021.174620
61. Hong H, Wang Y, Menard M, et al. Suppression of the JAK/STAT pathway inhibits neuroinflammation in the line 61-PFF mouse model of Parkinson's disease. *J Neuroinflammation*. 2024;21(1):216. doi:10.1186/s12974-024-03210-8
62. Hoffman O, Koehler J, Espina J, et al. Disease modification upon 2 weeks of tofacitinib treatment in a mouse model of chronic epilepsy. *Sci Transl Med*. 2025;17(790):eadt0527. doi:10.1126/scitranslmed.adt0527